BSc Fabian Steininger

Combining Electrochemistry with Optical Sensors; a New Avenue towards Active Sensors

MASTER'S THESIS

to achieve the university degree of

Diplom-Ingenieur

Master's degree programme: Technical Chemistry

submitted to

Graz University of Technology

Supervisors

Assoc. Prof. kand. Sergey Borisov

Institute for Analytical Chemistry and Food Chemistry
Technische Universität Graz

Asst. Prof. Klaus Koren

Center for Water Technology, Department of Biology
Aarhus University

Graz, May 2020

Statutory Declaration

I declare that I have authored this thesis independently, that I have not used other than the declared sources / resources, and that I have explicitly marked all material which has been quoted either literally or by content from the used sources. The text document uploaded to tugrazonline is identical to the present master‘s thesis.

Eidesstaatliche Erklärung

Ich erkläre an Eides statt, dass ich die vorliegende Arbeit selbstständig verfasst, andere als die angegebenen Quellen/Hilfsmittel nicht benutzt, und die den benutzten Quellen wörtlich und inhaltlich entnommenen Stellen als solche kenntlich gemacht habe. Das in TUGRAZonline hochgeladene Textdokument ist mit der vorliegenden Masterarbeit identisch.

May 27, 2020
Date


Signature

Danksagung

Auf diesem Wege möchte ich mich bei allen Personen bedanken, welche mich durch meine Studienzeit begleitet haben - ohne euch wäre nie so weit gekommen. An erster Stelle möchte ich mich bei Klaus bedanken. Danke für die Möglichkeit in Aarhus meine Masterarbeit zu machen, für die super Betreuung, Freundschaft und den ein oder anderen Klettertrip. Danke dass du mir immer mit Rat und Tat zur Seite gestanden bist. Du hast oft Sachen in mir gesehen die ich selbst nicht gesehen habe und mich ermutigt weiterzumachen wenn es mal nicht so gut lief.

Danke Berni, dass du mich zum Chemiestudium „überredet“ hast und mich auch von Anfang an ein bisschen an der Hand genommen hast – ohne dich wäre der Studienstart um einiges schwieriger für mich gewesen. Danke auch, dass du meinen Weg zum ACFC geleitet hast und mir dadurch die optische Sensorik nahe gebracht hast. In diesem Sinne möchte ich mich auch bei allen ACFC Mitgliedern für die schöne Zeit, Kaffeepausen (für mich ohne Kaffee) und Dachterrassenbiere während meines Bachelorlabors und meiner Oompa-Loompa Zeit bedanken. Insbesondere möchte ich auch Sergey danken, der meinen Auslandsaufenthalt in Dänemark möglich gemacht hat.

Ich möchte mich auch bei allen Leuten die ich in den 7 Monaten in Dänemark kennengelernt habe für die schöne Zeit bedanken. Tusind tak an die Gesamte Arbeitsgruppe für das angenehme Arbeitsklima, die kurzweiligen Mittagspausen und netten Gespräche. Danke Caro und Ronny, dass ihr uns von Anfang an so nett aufgenommen habt und auch für die unzähligen Stunden am Kickertisch (für alle Österreicher: Wuzeltisch), beim Ølsnedkeren und in der Boulderhalle.

Ein ganz großes Dankeschön möchte ich auch an meine Studienkollegen und Freunde in Graz richten. Danke Resi für die schöne Zeit in Dänemark und dass du immer ein offenes Ohr für mich gehabt hast wenn ich Probleme hatte - ich bin froh, dass wir diese Zeit gemeinsam erleben durften. Danke Felix und Simon für die beste WG die man sich vorstellen kann. Danke Flo, Anna, Feri, Vici, Jakob und allen anderen, dass ihr mich durch dieses Studium begleitet habt und es zu einer unvergesslichen Zeit gemacht haben – ohne euch wäre ich nicht da wo ich jetzt bin. Außerdem möchte ich mich auch noch bei meinen Freunden zuhause im Mühlviertel bedanken. Es ist schön, dass ich mich jedes Mal sofort wieder zuhause fühle auch wenn ich nicht mehr so oft nach Hause komme wie ich gerne wollen würde.

Der größte Dank jedoch gilt meiner Familie: Mama, Papa, Daniel, Martin, Oma und Opa. Danke, dass ihr immer für mich da wart und seid egal in welcher Situation. Danke Papa für deine Unterstützung in guten so wie in schlechten Zeiten. Danke Martin für deinen Rat und dass du immer an mich geglaubt hast. Danke Oma und Opa, dass ihr immer für mich da wart und wie Schutzengel über mir wacht. Danke Daniel, dass du immer mein großer Bruder und Vorbild warst und immer noch bist und auf mich aufgepasst hast. Danke Mama, dass du immer auf meiner Seite bist und auch wenn es manchmal schwer fällt mich gehen zu lassen, immer mich und meine Entscheidungen unterstützt. Auch wenn ich manchmal etwas zu neugierig bin und mir die ganze Welt anschauen möchte, so werde ich nie meine Wurzeln vergessen.

Danke euch allen, dass ihr einen Teil meines Weges mit mir gegangen seid!

Graz, May 27, 2020

Abstract

In this thesis a novel dynamic sensing platform for buffer capacity was developed based on the combination of optical pH sensors with electrochemical water splitting. The methodology was tested in several different buffer systems (MOPS, HEPES and carbonate) in a wide concentration range (2-100 mM) showing good reproducibility. The system was also used to determine the apparent pK_a of a buffer solution at present conditions (i.e. temperature and ionic strength). Practical application of the sensor was tested by measuring lake surface and pore water alkalinity.

Additionally, alternative methods for localized electrochemically induced pH shifting were investigated. "Electro acids/bases" which can reversibly capture and release protons in aqueous solution upon electrochemical stimulus have been previously shown to be able to induce localized pH gradients. In this thesis two quinone-based molecules, being possible candidates for reversible pH switching, were characterized electrochemically regarding their electrochemical reversibility and stability in aqueous solution.

Kurzfassung

Die Messung von chemischen Parametern ist unerlässlich für die chemische Industrie, Bioprozesstechnik und um biologische Prozesse besser verstehen zu können. Chemische Sensoren sind wichtige Werkzeuge, um eben diese Parameter messen zu können. Diese Sensoren werden meist nach dem grundlegendem Messprinzip (optisch, elektrochemisch, etc.) kategorisiert. Obwohl diese verschiedenen Messprinzipien oft miteinander verglichen werden, sind Sensoren welche verschiedene Methoden kombinieren zur Zeit noch eher selten. Die einzelnen Messtechniken haben bestimmte Vor- und Nachteile, jedoch könnte eine Kombination verschiedener Methoden neue Möglichkeiten eröffnen welche großes Potential haben. Im Zuge dieser Arbeit wurde ein neuartiger dynamischer Pufferkapazitätssensor entwickelt, basierend auf der Kombination von optischen pH Sensoren und elektrolytischer Wasserspaltung. Die Messmethode wurde anhand von verschiedenen Puffersystemen (MOPS, HEPES und Karbonat) in einem breiten Konzentrationsbereich (2-100 mM) getestet und wies eine gute Reproduzierbarkeit auf. Weiters, konnte das System verwendet werden um den tatsächlich vorherrschenden pK_s Wert einer Pufferlösung bei vorhandenen Bedingungen (Temperatur und Ionenstärke) zu messen. Als praktische Anwendung des Messsystems wurde die Alkalinität von Oberflächen- und Porenwassers eines Sees bestimmt.

Zusätzlich wurden Alternativmethoden zur lokalisierten elektrochemischen pH Änderung untersucht. Sogenannte Elektrosäuren/basen können in wässriger Lösung durch einen elektrochemischen Stimulus reversibel Protonen aufnehmen und wieder abgeben und dadurch einen örtlich konzentrierten pH Gradient erzeugen. Deswegen wurden im Zuge dieser Arbeit zwei chinon-basierte Moleküle elektrochemisch, in Hinsicht auf elektrochemische Reversibilität und Stabilität in wässrigen Lösungen, untersucht.

Contents

Part I.

Introduction

1. Scope of this Thesis

Chemical sensors are often classified by their mode of transduction. In other words, there can be optical, electrochemical, thermometric sensors which all sense the same analyte. Each method certainly have their advantages and disadvantages and while they are often compared, combinations of methods are rather scarce and synergies between different transducers are not exploited to the fullest. A recent review about coupling electrochemistry with fluorescence microscopy stated the following *"Although these two approaches (meaning optical and electrochemical) are most of the time compared, their combination instead may offer very promising synergistic opportunities."* [1].

In recent years research towards the combination of optical and electrochemical methods has gained increased attention and successful combination of the two has been presented in several fields. Examples include electrofluorochromic materials [2–5], redox microscopy [1] and spectroelectrochemical methods to follow fluorescence emission of redox-acitve molecules at screen printed electrodes [6]. Also, several sensing applications have been developed using combination approaches based on e.g. bipolar electrodes [7–10] or electrofluorochromic polymers [11].

The aim of this thesis was to develop a sensor combining electrochemical methods and optical sensors. More specifically, a novel dynamic sensor for buffer capacity was developed combining electrochemical water splitting and optical pH measurement in a flow cell. Water electrolysis was used to achieve a localized pH shift at the electrodes which was monitored using two optical pH sensors. The monitored change of pH at the electrodes during the application of an electrochemical potential is dependent on the intrinsic buffer capacity of the measured sample.

Redox induced pH shifting presents an interesting alternative to water electrolysis to achieve a localized pH change. This process requires so-called electro acids/bases which can reversibly capture and release protons and therefore alter the pH close to the electrodes. In this thesis two possible quinone-based candidates were characterized using cyclic voltammetry regarding electrochemical reversibility and stability in aqueous solution.

2. Theoretical Background

2.1. Buffer Capacity & Alkalinity

The following section is based on references [12–14]. All other sources will be referenced explicitly.

2.1.1. Fundamentals of Buffers

pH is one of the most fundamental analytes known. It is defined as the negative decadic logarithm of H^+ ion activity (equation 2.1).

$$pH = -\log(a_{H^+}) \tag{2.1}$$

It is a crucial parameter for many natural environments, biological fluids as well as industrial processes. Most of these systems rely on stable pH values to function at their optimum rate. Therefore, these systems often use chemical compounds which can uptake protons and hydroxyl ions and can therefore counteract drastic pH changes. These compounds are called *buffering agents* and can resist change in pH when a small amount of acid or base is added or the solution is diluted. Buffers consist of a weak acid (HA) and its conjugated base (A^-) or vice versa. This equilibrium can be described as

$$HA \rightleftharpoons H^+ + A^-$$

When acid (H^+) is added to the system the equilibrium is shifted to the protonated form of the buffer according to *Le Châtelier's principle*. Thus, the pH decrease of the solution is less severe compared to unbuffered solutions because a part of the added protons are bound by the buffer molecules. Similarly, the addition of base results in less pH increase due to the buffer reacting with the hydroxyl ion instead of the protons in solution and therefore inhibiting the neutralization reaction.

$$OH^- + HA \rightleftharpoons H_2O + A^-$$

For monobasic buffers which dissociate completely in aqueous solution the pH can be estimated by the *Henderson-Hasselbalch equation*

$$pH = pK_a + log\frac{[A^-]}{[HA]} + log\frac{f_{A^-}}{f_{HA}} - log\ a_{H_2O} \tag{2.2}$$

where $[A^-]$ and $[HA]$ are the basic and acidic form, respectively. f_{A^-} and f_{HA} are the activity coefficient of both forms and a_{H_2O} denotes the activity of water (constant). The titration of such a buffering agent is represented in Figure 2.1. Obviously, the buffer counteracts a pH change in both directions the most at its pK_a. Therefore, buffer solutions are usually prepared at pH $\approx$ $pK_a \pm 1$ for laboratory use.

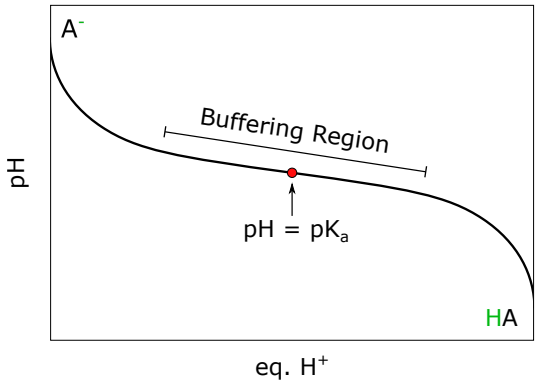

Figure 2.1.: Schematic titration curve of a monobasic buffering species.

Buffer capacity β describes the efficiency of the buffering agent to withstand pH change upon addition of acid (dc_a) or base (dc_b).

$$\beta = \left|\frac{dc_a}{d(pH)}\right| = \frac{dc_b}{d(pH)} \tag{2.3}$$

Since buffer capacity is always positive by convention, absolute values have to be considered when calculating the buffer capacity upon addition of acid. Buffer capacity is a derivative and it makes no difference whether the differential change in pH is the result of addition of acid or base. Buffer capacity can be split up in a series of terms

$$\beta_{tot} = \beta_{OH^-} + \beta_{H^+} + \sum \beta_i(\text{all weak acids and bases})$$

where β_i denotes the contribution of each buffering species in solution and β_{OH^-} and β_{H^+} usually correspond to the buffering capacity of water in aqueous solutions. However, if strong Arrhenius acids or bases are added an increase in the respective term is observed. Before only monobasic buffer species were discussed, however there are several buffers which have more than one pK_a values and are therefore able to uptake more than one proton. An example of this phenomenon is the phosphate buffer system (triprotic acid and conjugated base). Figure 2.2 shows the buffer capacity contribution of the phosphate buffer system, the buffer capacity contribution of water and the resulting total buffer capacity. In the phosphate system three distinct maxima can be seen which correspond to the pK_a values of the respective protonation/deprotonation steps. However, for $pK_a < 3$ or $pK_a > 11$ the maxima begin to converge with the contribution of H^+ and OH^- to form a single relative maximum.

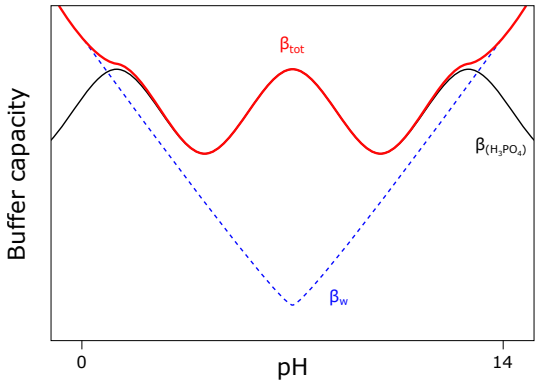

Figure 2.2.: Schematic representation of buffer capacity of the phosphate system. Contribution of H^+ and OH^- are shown as β_w (blue), the contribution of the phosphate system is shown as $\beta_{(H_3PO_4)}$ (black) and the resulting buffer capacity is shown as β_{tot} (red).

Alkalinity is an alternative approach to assess the effectiveness of a buffer solution. It measures the ability of the buffer solution to neutralize titrated acid until a specific pH value is reached. Thus, alkalinity describes the total amount of alkaline substances which can be protonated in that pH-range. *Total alkalinity* A_T (titration to pH 4.5) describes the sum of all basic compounds which can uptake protons from the titrant.

$$\begin{aligned} A_T = {} & [HCO_3^-] + 2[CO_3^{2-}] + [B(OH)_4^-] + [OH^-] + [HPO_4^{2-}] \\ & + 2[PO_4^{3-}] + [SiO(OH)_3^-] + [NH_3] + [HS^-] + \dots \\ & - [H^+]_F - [HSO_4^-] - [H_3PO_4] - \dots \end{aligned} \tag{2.4}$$

Here the ellipses stand for minor acid or base species which usually occur only in very small amounts and can therefore be neglected. $[H^+]_F$ describes the free concentration of hydrogen

ions and in combination with other acids in solution leads to a decrease in alkalinity as they act as a proton source. This equation is often simplified to a system that only considers the carbonate system, hydroxyl ions and boric acid as they are usually the major contributors to total buffer capacity in natural samples and smaller contributing species like phosphates, silicates and ammonia are often neglected. However, in several natural samples (e.g. anoxic waters) they may show significant contribution [15].

Nevertheless, it is undeniable that in most natural samples carbonate and bicarbonate are the most prominent contributors to alkalinity. Therefore, in samples at pH > 8.3 besides total alkalinity also the *carbonate alkalinity* (or phenolphthalein alkalinity) is assessed by titrating to pH 8.3. At this pH all carbonate is converted to bicarbonate.

2.1.2. Importance of pH Buffers

Stable pH environments are of vital importance to biological systems and therefore essential in life-sciences, medicine and environmental and marine sciences. Furthermore, reaction rates of several chemical and biochemical processes depend on pH and therefore it is also important in chemical and biotechnological process control in industry.

In the human body acid-base homeostasis is of utmost importance. The pH of blood is kept remarkably constant and tightly regulated in a pH range of 7.35 to 7.45 and even minor deviations ($\pm$ 0.3 pH is considered an extreme change from a physiological viewpoint) can have severe cardiovascular, respiratory , neurologic and metabolic consequences [16]. Generally, acidic metabolites are produced in greater quantities than basic ones, with CO_2 being predominant. Those metabolites are dealt with by various buffer systems (e.g. bicarbonate buffer, phosphate buffer, protein buffer, hemoglobin/oxyhemoglobin, etc.). Eukaryotic cells are highly compartmentalized with each compartment having distinct environments ensuring optimal operation conditions for metabolic processes. These compartments maintain a certain pH by their inherent buffering capacity which reduces the acute effect of rapid, localized pH swings. However, due to their finite nature those buffering systems are not powerful enough to withstand sustained stress [17].

Also in natural environments pH buffers play a key role to maintain stability. Changes in pH in soil are accompanied by changes in nutrient solubility, microbial activity, mineralization, decomposition etc. Buffering species prevent drastic changes in pH that might be harmful to plants, microorganisms and the ecosystem in general. Acidification of soil can be the result of many naturally occurring processes like nitrification, sulfur oxidation, etc. but is also observed due to human impact (e.g. fertilization, acid rain, etc.) [18]. This decrease in soil pH can lead to limited availability of nutrients like calcium, magnesium and potassium and increased

solubility and therefore increased availability of elements toxic to plants like aluminium. This can damage root tips and constrain root elongation and inhibit plant growth [19]. Besides soil, stable pH environments are also crucial for aquatic organisms like algae [20], fish and other marine organisms [21].

2.1.3. Measurement Techniques

To assess buffer capacity or any form of alkalinity some sort of titration has to be performed. Historically, alkalinity titrations were performed using strong acids like HCl or H_2SO_4 and the indicator dyes phenolphthalein and methyl orange. The pK_a value of these dyes correspond quite well with the pH value at which carbonate (phenolphthalein) and bicarbonate and other minor buffering species (methyl orange) are exhausted. This is also the reason why carbonate and total alkalinity are often referred to as phenolphthalein and methyl orange alkalinity. While these methods are still being used today, nowadays more popular methods include colorimetric [22] and potentiometric acid-base titrations [23]. Besides titration-based techniques various other methods to measure alkalinity have been investigated, including ion-selective electrodes [24] and two-dimensional imaging using DET techniques [25].

It has to be stated that all these methods are ex-situ measurements and therefore when dealing with real samples possible deviations due to different CO_2 partial pressures throughout the manipulation during sampling, transport and measuring procedures can lead to loss of integrity in the sample due to re-equilibration with atmospheric CO_2 which is often quite different from the original in-situ value. This is also the reason why it is especially hard to compare results of in-situ methods with traditional on-site measurements, which generally show higher levels of carbonate most likely due to the equilibration with atmospheric CO_2 [26]. Therefore, research towards in-situ measuring methods has gained increasing attention lately. Wiorek et al. presented a alkalinity measuring platform based on polyaniline films acting as electrochemical proton pump for acidification of the sample which allowed in-situ measurements of alkalinity in a small measurement chamber [27].

Among these alternative methods also some optical sensing techniques can be found, which are mostly based on optical pH indicators incorporated in hydrogel matrices. Mistlberger et al. presented a titration-free non-equilibrium based system using an active sensing principle in which the indicator can be activated by irradiation with UV light [28]. Furthermore, with increasing demand for in-situ measurements research in portable, easy-to-use devices has gradually increased over the last years [29].

2.2. Local pH Change Methods

Besides a few exceptions, most buffer capacity or alkalinity measuring techniques require the introduction of a strong acid or base. Conventionally this is achieved by the addition of either hydrochloric acid or sulfuric acid. Here it is crucial that the exact concentration is known, which is usually achieved by titrating the used acid with a standard solution of Na_2CO_3.

2.2.1. Water Electrolysis

Alternatively, acid or base can be introduced electrochemically by in-situ production of H^+ and OH^-. Application of an electric potential in aqueous solution causes cations, including H^+, to move towards the negative electrode (cathode) and anions, including OH^-, to move towards the positive electrode (anode). This heterogeneous reactions take place at the boundary layer between electrolyte and the respective electrode:

$$\begin{aligned} Anode(oxidation): &\quad H_2O(l) \quad \rightleftharpoons \quad 2H^+(aq) \; + \; \tfrac{1}{2}O_2(g) \; + \; 2e^- \\ Cathode(reduction): &\quad 2H_2O(l) \; + \; 2e^- \quad \rightleftharpoons \quad 2OH^-(aq) \; + \; H_2(g) \\ \hline Overall: &\quad H_2O(l) \quad \rightleftharpoons \quad \tfrac{1}{2}O_2(g) \; + \; H_2(g) \end{aligned} \tag{2.5}$$

When the electrode compartments are separated (either by distance or by a suitable porous membrane) a significant increase or decrease of pH in the respective compartment, depending on the applied potential, is observed as ions are produced or consumed at the electrode surface. The thermodynamic requirement for the electrolysis of water is a potential difference of 1.23 V. At this potential water electrolysis is kinetically reversible and both oxygen and hydrogen evolution reactions barely proceed. Therefore, in order to drive the reaction at a significant rate a certain overpotential must be applied. The actual potential required is determined by localized concentration of reactants and products (i.e. local pH influences the required potential), surface area loss of the electrode due to coverage by gas bubbles, temperature and gas partial pressures [30]. Consequently, modern electrolyzers are usually operated at a voltage of 1.8-2.0 V. The focus of research to increase reaction rate and reduce the onset potential of water electrolysis revolves around the development of new electro-catalysts suitable for hydrogen evolution reaction (HER) and oxygen evolution reaction (OER) [31–34]. Additionally, variations in local pH in both electrode compartments also change the required potentials for

HER and OER. Generally, with increasing pH decreased potentials for the half reactions can be observed.

$$
\begin{aligned}
&\text{In acidic electrolyte:} \\
Anode: \quad & H_2O(l) \quad \rightleftharpoons \quad 2H^+(aq) \; + \; \tfrac{1}{2}O_2(g) \; + \; 2e^- && E_a^0 = 1.23\ V \\
Cathode: \quad & 2H^+(aq) \; + \; 2e^- \quad \rightleftharpoons \quad H_2(g) && E_c^0 = 0.0\ V
\end{aligned}
\tag{2.6}
$$

$$
\begin{aligned}
&\text{In alkaline electrolyte:} \\
Anode: \quad & 2OH^-(aq) \quad \rightleftharpoons \quad H_2O(l) \; + \; \tfrac{1}{2}O_2(g) \; + \; 2e^- && E_a^0 = 0.40\ V \\
Cathode: \quad & 2H_2O(l) \; + \; 2e^- \quad \rightleftharpoons \quad H_2(g) \; + \; 2OH^-(aq) && E_c^0 = -0.83\ V
\end{aligned}
$$

Consequently, if the anode reaction was forced to run at pH 14 and the cathode reaction was run at pH 0 a significantly lower onset voltage could be required to perform water electrolysis. However, the acidic and alkaline conditions must be maintained throughout the electrolysis process, which requires further input of energy [35].

In most applications like hydrogen gas production the local pH shift at the electrodes during water electrolysis is only a side-effect and the main focus is the reaction-product itself. However, water electrolysis has also seen increased use in the form of a controllable proton pump in various applications. It is an attractive alternative to conventional acidification and alkalinization methods because as long as some sort of electrolyte is present in the sample (in physiological or marine sample usually adequate amounts of various salts are present) it does not require additional chemicals to be added to the sample. Water splitting has been used to establish pH gradients to regulate pH in microfluidics [36–38], to generate pH gradients in microfluidic channels for isoelectric focussing [39] and to control and monitor reactivity at surfaces [40].

2.2.2. Electro-acid/base mediated pH Change

Alternatively, pH gradients can be electrochemically generated by the use of electro-acids/bases. These molecules are able to capture and release protons reversibly upon electrochemical stimulus. A prominent example for such molecules are quinones. Quinones are organic aromatic molecules bearing two ketone groups, which can be chemically or electrochemically reduced to yield the hydroquinone form. When performed in aqueous solution, the oxidation or reduction of quinones is thereby accompanied by a change in hydrogen ion concentration in solution. This change highly depends on the concentration of the quinone solution and the electrochemical reaction rate (i.e. it is therefore dependent on various parameters like electrode material, applied potential, cell resistance, etc.).

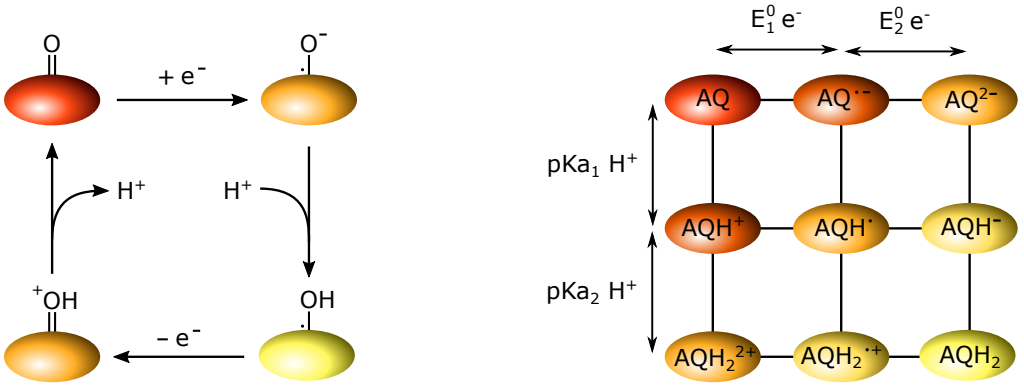

Figure 2.3.: General quinone associated redox process of one ketone group (left) and complete redox system ("scheme of squares") of anthraquinone (right). Adapted from [41].

Figure 2.3 shows the general redox process of one ketone group of a quinone and a complete quinone redox system using anthraquinone in the form of a "scheme of squares" as an example.

The dominant mechanistic pathways of the reduction highly depends on the initial pH of the sample solution as can be seen in Figure 2.4. Due to high abundance of protons in low pH solutions the protonation step usually happens before the electron transfer. With increasing pH electrochemical processes tend to happen before the protonation step and at very high pH values the protonation step is suppressed due to very low levels of hydrogen-ions in solution. Quinones are one of the most studied electroactive molecules and therefore a prominent choice for redox induced pH-switching in bulk solutions in potentiostatic fashion [42, 43].

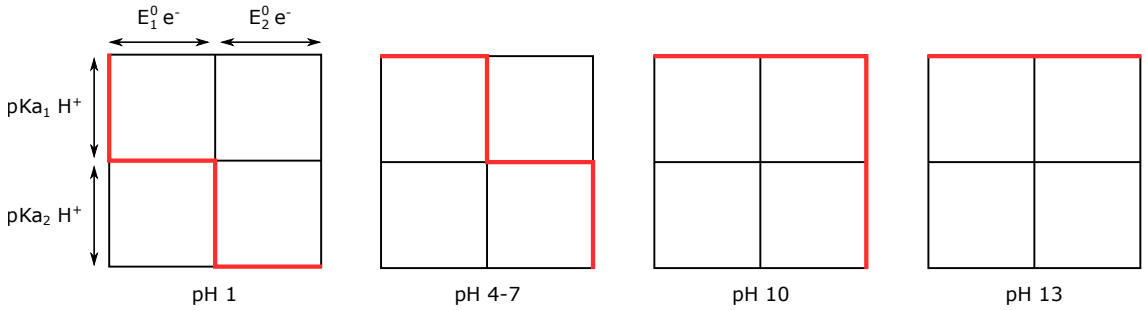

Figure 2.4.: "Scheme of squares" of the reduction of anthraquinone-2,6-disulfonate $2\,H^+$, $2\,e^-$ redox system at various pH values. Adapted from [44].

While electro acid/base mediated alteration of local pH in potentiostatic mode allows easy manipulation of pH close to the electrodes, precise spatial control is hard to achieve. By using galvanostatic techniques the current passed through the electrodes can be controlled more readily resulting in a more defined spatial manipulation of pH [45].

Another example of molecules capable of redox induced pH switching are electroactive polymers

like polyaniline, which is a pH sensitive polymer that converts to its non-conductive form at pH 3 [46]. Therefore, it can be used for controlled proton release upon anodic potentials in aqueous solutions [27].

2.3. Electrochemical Methods

In order to facilitate redox induced localized pH change fundamental understanding about electrochemistry and electrochemical methods is imperative. Furthermore, electrochemical characterization methods allow to assess various candidates of electro acids/bases regarding their electrochemical reversibility and stability in aqueous solution.

The following section is based on references [47–49]. All other sources will be referenced explicitly.

2.3.1. Fundamentals of Electrochemistry

Electrochemistry describes processes related to electron transfer reactions at the interface of an electronic conductor (*electrode*) and an ionic conductor (*electrolyte*). In the electrode charge is transported by electron (and hole) movement, while in the electrolyte charges are carried by the movement of ionic species (e.g. H^+, Na^+, Cl^-, etc.). Electrochemical processes are studied in *electrochemical cells*, which generally consist of two or three electrodes separated by at least one electrolyte phase. The over-all reaction taking place in the cell is the sum of two *half-reactions*, which describe the actual chemical processes happening at the electrodes. The electrode at which the reaction of interest occurs is called *working electrode*. In order to control the reaction at the working electrode, the other half of the cell is standardized by using a *reference electrode* with constant composition and a stable and well-known electrode potential. The potential is then said to be controlled with respect to the chosen reference electrode.

In this *two-electrode* setup the potential across the whole cell is measured, including contributions of the reference electrode/electrolyte interface. This setup can be used when the potential control of the working electrode is not crucial and the interfacial potential across the whole cell is investigated. However, if precise control of potential or current at the working electrode is of importance a third electrode (*auxiliary/counter electrode*) can be introduced (*three-electrode setup*). This electrode is used to close the current circuit in the electrochemical cell with the working electrode. Thus, the current flow in the reference electrode can be kept close to zero and therefore a constant potential can be maintained under changing experimental conditions.

Depending on the applied potential the energy of electrons can be increased or decreased. At a certain potential the energy may be shifted enough to facilitate electron flow in the form of heterogeneous electron transfer from the electrode to the solution (*reduction*) or vice versa (*oxidation*). When a reversible system with fast kinetics is investigated the *Nernst equation* solves the potential of the electrochemical cell or the half-reaction (see equation 2.20).

2.3.2. Cyclic Voltammetry

Cyclic voltammetry (CV) is a powerful technique and one of the most widely practised electrochemical methods, which is commonly employed to investigate redox processes of molecular species. It is a *potential sweep method*, where the voltage is ramped linearly with time at a certain *scan-rate* (mV/s) and reversed at the *vertex potential*. These parameters have to be adapted to each experiment because some diffusion limited processes may proceed very slow and require low scan rates in order to get observable results. If the scan rate is too fast, the electron exchange process may not occur in that time scale and will not be visible. During the experiment the current flowing through the working electrode is recorded and plotted versus potential (*voltammogram*). The observed voltammogram mainly depends on the standard electrochemical rate constant k^0, the formal potential of the redox couple, the diffusion coefficients of the oxidized and reduced species and the scan rate. This potential sweep and the resulting cyclic voltammogram and concentration profiles are exemplified in Figure 2.5.

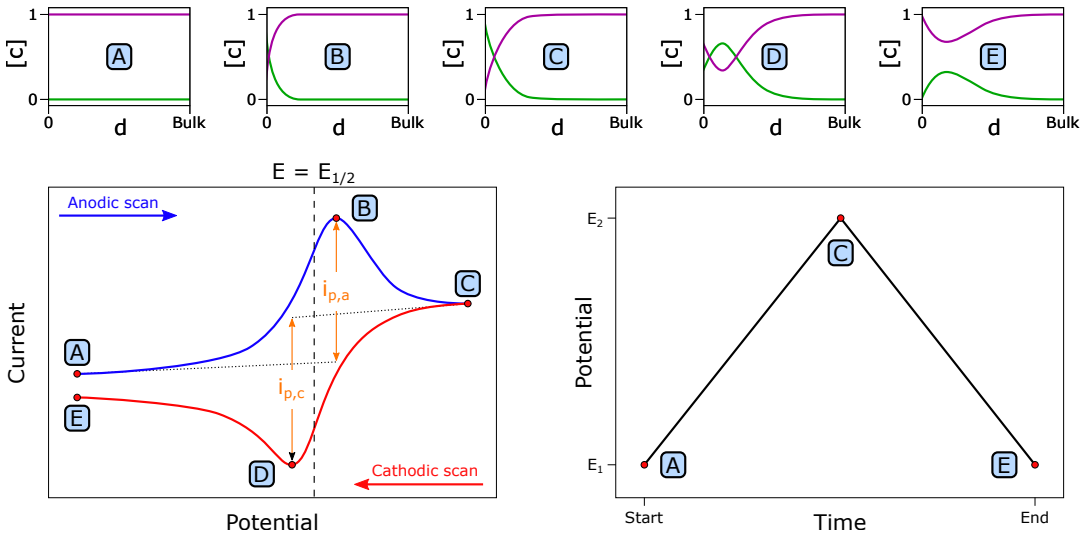

Figure 2.5.: Schematic cyclic voltammogram of a reversible redox couple (left) and the applied potential as a function of time (right). The resulting concentration profiles for oxidized (green) and reduced form (purple) of the redox couple are shown as a function of the distance from the electrode (top). Adapted from [50].

At the beginning of the experiment only the reduced (R) and no oxidized (O) form is present (A). A small increase in current can be observed while scanning in anodic direction. This is mainly attributed to non-faradaic currents which are independent from the electrochemical reaction itself and can be caused by formation of the electrical double layer, migration or reorientation of solvent molecules. This *background-current* is usually observed throughout the experiment. As the scan moves in anodic direction a faradaic current attributed to the redox reaction begins to flow close to the equilibrium potential of the oxidation reaction. The current peaks (B) and decreases again due to fast depletion of R and therefore lack of available reactant at the electrode.

The scan direction is reversed at the vertex potential (C) and the current decreases. Here the concentration of R at the electrode is close to zero because of the growing diffusion layer, the electrode kinetics are under diffusion control. As the potential is driven to lower potentials the reduction reaction occurs and the current peaks (D). Again, a depletion of reactant is observed and the current is dictated by delivery of additional O by diffusion from the bulk solution. At the end point of the scan (E) the concentration of O is close to zero at the electrode surface and that of R has almost replenished to the original value.

When investigating the reversibility of a redox process it has to be distinguished between chemical and electrochemical reversibility. *Chemical reversibility* refers to the analyte being stable upon reduction and if it can be subsequently reoxidized. Some analytes may undergo irreversible changes (ligand loss or degradation) during the first part of the CV and therefore only a reduction peak without the associated oxidation peak, or vice versa, may be observed. On the other hand, *electrochemical reversibility* refers to the electron transfer kinetics (described by the electrochemical rate constant k^0) of the analyte at the electrode surface in relation to mass transport to the electrode (m_T). If the energy barrier for electron transfer is low (fast kinetics, $k^0 \gg m_T$) the Nernst equilibrium is established almost immediately when the equilibrium potential for a redox process is reached and the system is said to be electrochemically reversible. Contrary, if the energy barrier is high (slow kinetics, $k^0 \ll m_T$), more potential-shift is needed to drive the reaction towards oxidation or reduction (electrochemical irreversibility). This results in a drawn-out voltammogram with broadened peaks and increased peak separation due to greater overpotential needed for the same rate of electron transfer.

Another important parameter in cyclic voltammetry is peak height. For diffusion controlled processes the peak current i_p is described by the *Randles-Sevčik equation*

$$i_p = 0.4463 \left(\frac{F^3}{RT}\right)^{1/2} z^{3/2}\, A D_0^{1/2}\, c_0^*\, v^{1/2} \tag{2.7}$$

where F is the Faraday constant, R is the gas constant, T is the temperature in Kelvin, z is the number of electrons transferred in the redox event, A is the electrode area, D_0 is the

diffusion coefficient, c_0^* is the bulk concentration and v is the scan rate. This equation predicts that the peak current is proportional to the square root of the scan rate for reversible diffusion controlled redox couples.

In general, the reversibility of a redox couple should can be assessed by the following characteristics:

- Peak separation of $\Delta E_p = E_{p,a} - E_{p,c} = 59\ mV$ for single electron processes, which is independent of scan rate (at 25 °C).
- The formal potential which is located midway between peak potential and half-peak potential can be described as $|E_p - E_{p/2}| = \frac{59}{z}\ mV$ (at 25 °C)
- Peak current ratio of the oxidation and reduction reaction is unity.
- Peak currents are proportional to the square root of the scan rate (equation 2.7).

2.3.3. Chronoamperometry

Chronoamperometry is a *potential step method*, where the current-time behaviour of an electrochemical cell is recorded upon a step change in potential in an unstirred solution. A schematic representation of this type of experiment and the resulting concentration profiles are depicted in Figure 2.6.

Here a system is described in which the investigated molecule is electrochemically inactive at a certain potential E_1 and therefore no faradaic processes occur (A). As soon as the potential is stepped to E_2 where the molecule is oxidized rapidly, the concentration of the reduced species in the vicinity of the electrode drops close to zero and a peak in current is recorded (B). Due to the instant nature of this event (fast kinetics) a large amount of current is required to drive this reaction and current continues to flow to maintain the oxidized state of the molecule at the electrode. Thus, a concentration gradient is generated supplying reactant from the bulk to the electrode, where it immediately reacts due to the applied potential. The recorded current is therefore proportional to the concentration gradient at the electrode surface. However, this continuous flux to the electrode creates a zone of depletion which is growing with time and causing the current to decrease (C-E).

The measured current also depends on the applied potential E_2. If the applied voltage has not fully reached the equilibrium potential of the oxidation or reduction reaction the redox process at the electrode is not so dominant, so that some reduced species can coexist at the electrode surface, a smaller gradient and therefore a smaller current is observed. However, once the equilibrium potential is reached every reduced molecule reaching the electrode is immediately

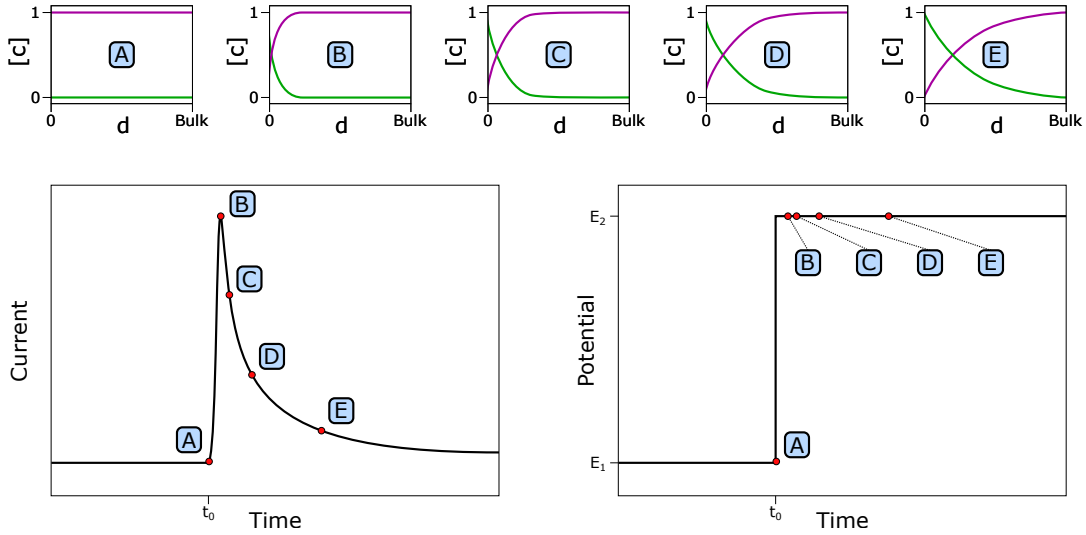

Figure 2.6.: Schematic chronoamperometry experiment at a planar electrode. Applied potential waveform (right) and current response (left). The resulting concentration profiles for oxidized (green) and reduced form (purple) in vicinity of the electrode are shown as a function of the distance from the electrode (top).

oxidized, resulting in a greater flux of reactant from the bulk to the electrode. Even if the potential would be increased to higher levels the flux of reactant and current would be the same, because the mass transport to the electrode is limited by diffusion.

The current response to a potential step over a certain time under conditions of large overpotential can be described by the *Cottrell equation*

$$i(t) = \frac{zFAD_0^{1/2}c_0^*}{(\pi t)^{1/2}} \tag{2.8}$$

where z is the number of electrons participating in the redox process, F is the Faraday constant, A is the area of the planar electrode, D_0 is the diffusion coefficient of the electroactive species, c_0 is the initial/bulk concentration and t is time. However, this equation is only valid at high overpotentials in order to ensure rapid depletion of the electroactive species making the reaction controlled by diffusion.

2.4. Fundamentals of Luminescence

Buffer capacity measurements require some sort of pH measurement in order to follow the induced localized pH shift. In the scope of this thesis optical sensors are used to monitor this pH change. These sensors are based on variations of luminescence processes (e.g. fluorescence or phosphorescence) upon interaction with the analyte (in this case H^+). The following section gives a brief introduction about Luminescence and is based on references [51, 52]. All other sources will be referenced explicitly.

Luminescence is the emission of light in the form of ultraviolet, visible or infrared photons from an electronically exited species. Luminescent compounds are generally divided into three categories: organic compounds (aromatic hydrocarbons, fluoresceins, rhodamins, amino acids, etc.), inorganic compounds (lanthanide ions, doped glasses, crystals, etc.) and organometallic compounds (ruthenium complexes, lanthanide ion complexes, complexes with fluoregenic agents, etc.). Figure 2.7 shows the possible physical effects of the interaction of light with matter. Depending on the mode of excitation it can be distinguished between different types of luminescence (absorption of light, electrical energy, ultrasound, etc.). Fluorescence and phosphorescence are two particular cases of luminescence. The energy for the excitation process is supplied by the absorption of photons and the de-excitation is accompanied by the emission of light. This phenomenon is called photoluminescence. In the scope of this thesis the focus will be on the absorption of light and the subsequent processes.

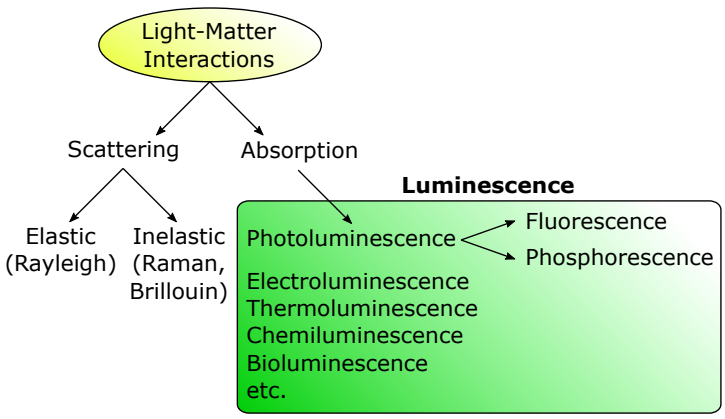

Figure 2.7.: Light-matter interactions.

2.4.1. Absorption

During absorption of a photon an electron is promoted from an orbital of a molecule in the ground state to an energetically higher unoccupied orbital. Depending on the molecular orbitals

involved in the excitation process, different transitions can take place. In most cases there are several possible transitions a molecule can undergo, depending on the energy and therefore wavelength of the electromagnetic radiation used to excite the molecule. Figure 2.8 illustrates the energy levels and all possible transitions of a formaldehyde molecule. Electrons from σ and π molecular orbitals of the carbonyl double bond, as well as the electron lone pairs of the oxygen can partake in the excitation process.

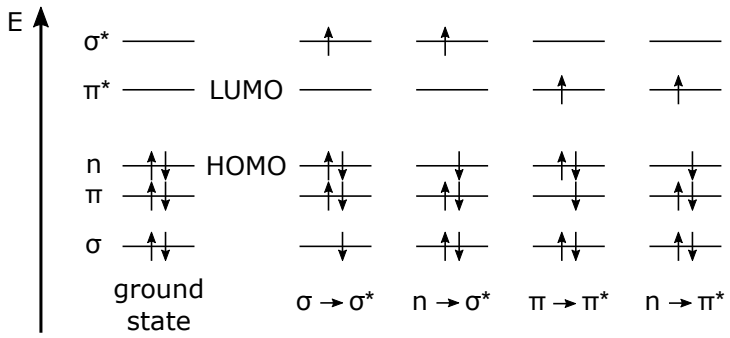

Figure 2.8.: Energy levels and possible transitions of a formaldehyde molecule.

Depending on the potential energy difference of the two involved molecular orbitals different amounts of energy and therefore different wavelengths are required for excitation. The corresponding energy for those transitions are in following order:

$$n \rightarrow \pi^* \ < \ \pi \rightarrow \pi^* \ < \ n \rightarrow \sigma^* \ < \ \sigma \rightarrow \pi^* \ < \ \sigma \rightarrow \sigma^* \tag{2.9}$$

However, when light in the UV-visible range is used to excite a molecule there are mainly two transitions to be observed: $\pi \rightarrow \pi^*$ and $n \rightarrow \pi^*$. Other transitions usually take place at higher energies and thus lower wavelengths. Increasing the conjugated π-system decreases the required energy for $\pi \rightarrow \pi^*$ transition, leading to a bathochromic shift in the absorption spectrum.

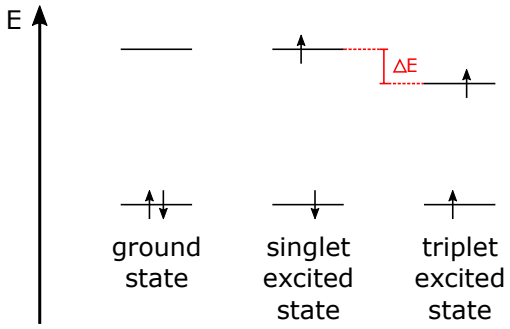

Figure 2.9.: Energetic differences of singlet and triplet state.

The most important types of orbitals are the Highest Occupied Molecular Orbital (HOMO) and the Lowest Unoccupied Molecular Orbital (LUMO), which both refer to the ground state of the molecule. Most commonly, a electronic transition corresponds to the promotion of an electron from the highest occupied orbital to an unoccupied orbital of higher energy. During this transition from ground to excited state the spin of the electrons usually remains the same, so that the total spin quantum number remains zero ($S = \sum s_i$ with $s_i = +\frac{1}{2}$ or $-\frac{1}{2}$). Since the multiplicity $M = 2S + 1$ of ground and excited state is 1, they are referred to as *singlet states*. Besides singlet-singlet transitions a molecule may also undergo a conversion where the promoted electron has changed its spin. This results in two electrons with parallel spins and therefore a total spin quantum number of one and multiplicity of three. This state corresponds to three states of equal energy and is called *triple state*. *Hund's rule* states that the triplet state is lower in energy than the singlet state of the same configuration (Figure 2.9).

The efficiency of light absorption by an absorbing medium at a given wavelength is described by the absorbance $A(\lambda)$ or the transmittance $T(\lambda)$, defined as

$$A(\lambda) = log\frac{I_\lambda^0}{I_\lambda} = -logT(\lambda) \tag{2.10}$$

where I_λ^0 and I_λ represent the intensity of the light beams entering and leaving the absorbing medium, respectively. In dilute solutions the absorbance follows *Beer-Lambert's law*

$$A(\lambda) = log\frac{I_\lambda^0}{I_\lambda} = \varepsilon(\lambda)lc \tag{2.11}$$

where ε is the *molar absorption coefficient* (L mol^{-1} cm^{-1}), c is the concentration (mol L^{-1}) and l is the absorption pathlength of the medium (cm). Deviations from the linear dependence of absorbance on concentration according to the Beer-Lambert Law can be observed due to aggregation at high concentrations or presence of other absorbing species. Classical theory states that molecular absorption of light and therefore ε depends on the *oscillator strength* of a molecule, which can be considered as an oscillating dipole. In quantum mechanics the *transient moment* describes the transient dipole resulting from the displacement of charges during transition. This is especially important for experiments carried out with polarized light, since molecules whose absorption transition moments are parallel to the vector of the linear polarized light are preferentially excited.

Selection Rules

For absorption transitions there a two main selection rules, determining if a transition is allowed.

Spin-forbidden transitions: While transitions between states with the same multiplicity (i.e. singlet-singlet, triplet-triplet) are allowed, transitions between states with different multiplicity (i.e. singlet-triplet, triplet-singlet) are forbidden. Nevertheless, weak interactions between states of different multiplicities can always be observed due to spin-orbit coupling. Thus, singlet wavefunctions always contain a small fraction of triplet wavefunctions and vice versa. While showing only very small absorption coefficients these transitions can still be observed.

Symmetry-forbidden transitions: Electronic transitions that conserve parity (symmetric or antisymmetric) with respect to the inversion centre are forbidden (*Laporte rule*). However, also symmetry forbidden transitions can be witnessed due to molecular vibrations, which cause some errors in perfect symmetry (vibronic coupling).

2.4.2. Franck-Condon Principle

The Born-Oppenheimer approximation states that the motion of electrons are much more rapid compared to the movements of the heavy nuclei. Therefore, atoms can be considered stationary during the fast excitation process of an electron to a molecular orbital of higher energy (10^{-15} s). As a result the Franck-Condon principle states that electronic transitions are likely to occur without changes in the positions of nuclei in a molecule. Figure 2.10 illustrates the potential energy as a function of the nuclear configuration.

It shows *vertical transitions* which results in the so called *Franck-Condon states*. In classical theory, this transition occurs when the distances between the nuclei are equal to the equilibrium bond lengths of the molecule in the ground state. When the vertical line intersects with the Morse potential of the lowest excited state, the transition terminates and the excited molecule begins to vibrate at the frequency corresponding to the energy of the excited vibrational state. Quantum mechanically, the transition takes place from the lowest vibrational state of the ground state to the vibrational state of the excited state which most resembles the wave function of the ground state. According to the Boltzmann distribution, most molecules are in the lowest vibrational level of the ground state at room temperature. The purely electronic transition is a 0-0 transition to the lowest vibrational level of the excited state. The intensities of the transitions depend on the relative shape and position of the potential energy curves.

The width of the resulting absorption bands depends on two factors: *Homogeneous broadening* occurs because there are several vibrational sublevels present in each electronic state. *Inhomogeneous broadening* is observed due to fluctuations of the structure of the solvation sphere surrounding the chromophore in solution.

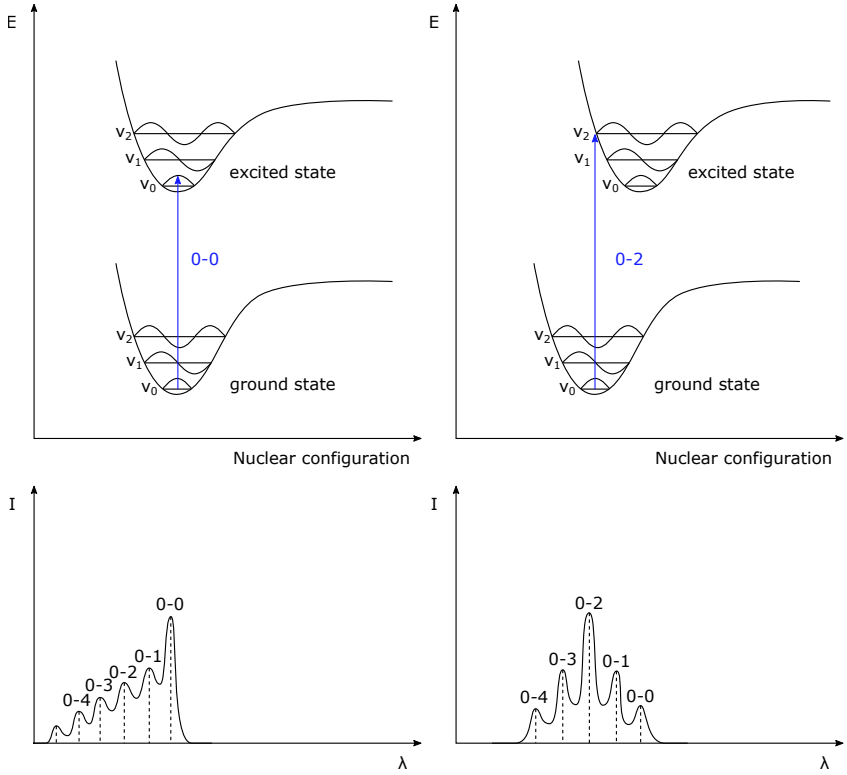

Figure 2.10.: Franck-Condon principle. Top: Potential energy diagrams with vertical transitions. Bottom: Resulting shape of absorption bands (dashed lines represent absorption lines in gas phase).

2.4.3. Transitions between Electronic States

From the excited state there are several possible pathways for the molecule to return to it's ground state. The *Perrin-Jablonski diagram* (Figure 2.11) illustrates all important transition which can take place upon promotion of an electron. The singlet electronic states are denoted as S_0, S_1, etc. and the triplet electronic states as T_1, T_2, etc. The possible de-excitation processes show different characteristic times (Table 2.1) and are explained in detail in the following paragraphs.

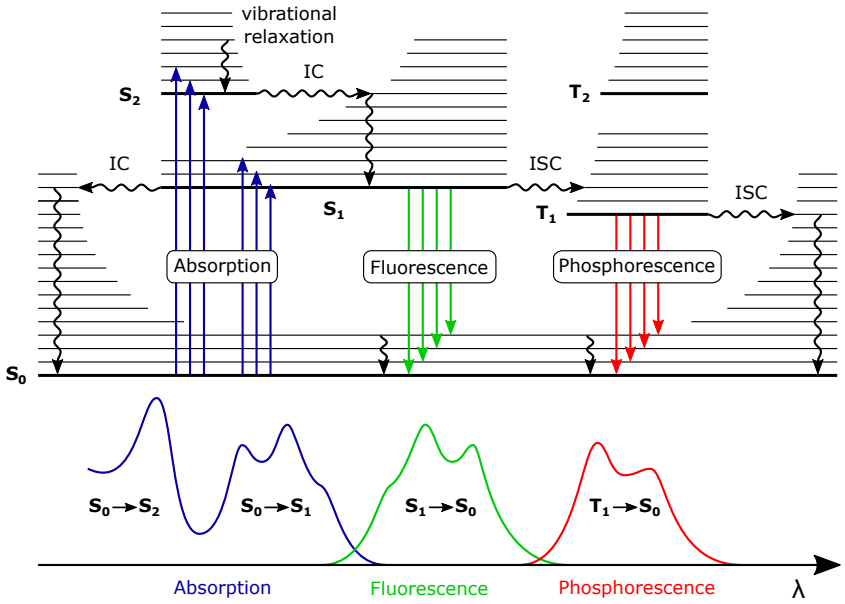

Figure 2.11.: Top: Perrin-Jablonski diagram showing all important transitions between excitation and subsequent de-excitation. Bottom: Relative positions of absorption, fluorescence and phosphorescence spectra.

Internal Conversion and Vibrational Relaxation

Internal conversion (IC) describes a non-radiative transition between two electronic states with the same spin multiplicity. In solution it is accompanied by vibrational relaxation to the lowest vibration level of the final electronic state (thermally equilibrated S_1). This vibrational relaxation takes place in a time scale of 10^{-13}-10^{-11} s. Excess energy resulting from this relaxation process is transferred to the surrounding solvent molecules. In general, internal conversion from S_1 to S_0 is possible, however since the energy gap between those singlet states is much larger and therefore the transition less efficient. Internal conversion from S_1 to S_0 can compete with photon emission (fluorescence) and intersystem crossing to the triplet state, followed by photon emission (phosphorescence).

Fluorescence

Relaxation from S_1 to S_0 accompanied by the emission of photons is called fluorescence. *Kasha's rule* states, that photon emission occurs only with appreciable yield from the lowest excited state of a given multiplicity. Therefore, besides a few exceptions, fluorescence emission usually occurs from S_1 and is thus independent on the excitation wavelength [53]. Because the excitation process does not greatly change the nuclear geometry the spacing between the vibrational levels of the excited and ground state are very similar. Consequently, the emission spectrum is typically a mirror image of the absorption spectrum of the S_0 to S_1 transition (*mirror-image rule*). However, fluorescence emission is generally located at higher wavelengths compared to absorption. This is due to the energy loss due to vibrational relaxation from higher vibrational levels of the excited singlet states to the thermally equilibrated excited state and was first observed by George G. Stokes [54]. The gap between the maximum of the first absorption band and the maximum of the fluorescence band is thus called *Stokes hift*. Usually, absorption and fluorescence spectrum partly overlap meaning that a fraction of light is emitted at shorter wavelengths than the absorbed light. This *energy defect* can be described by the fact that at room temperature a small part of the molecules are at higher vibrational level of the ground state. The population of the vibrational levels can be described by the *Boltzmann equation* (Equation 2.12).

$$\frac{N_1}{N_0} = e^{-\left(\frac{E_1 - E_0}{kT}\right)} \tag{2.12}$$

N_1 and N_0 are the number of molecules in vibrational level one and two and E_1 and E_0 describe the corresponding energies. k is the Boltzmann constant and T denotes the temperature in Kelvin. With decreasing temperatures this deviation of the Stokes law can be minimized.

The emission of photons happens on a similar time-scale like the absorption of photons (10^{-15} s) but the molecule stays in the excited state for a short period (10^{-11}-10^{-7} s) before relaxation happens, which is referred to as *fluorescence lifetime* of the excited state.

Intersystem Crossing

Intersystem crossing is a non-radiative transition that can occur during the lifetime of the excited singlet state S_1. It describes the transition between two isoenergetic vibrational levels of electronic states with different spin multiplicities (e.g. $S_1 \rightarrow T_n$), followed by rapid vibrational relaxation to the lowest vibrational level of the final electronic state. Intersystem crossing may compete with other de-excitation processes like fluorescence and internal conversion $S_1 \rightarrow S_0$.

This process is in principle spin-forbidden but can be possible due to spin-orbit coupling. Spin orbit coupling is the interaction of the spin-magnetic moment (produced by the rotation of the electron around its own axis) and the orbital magnetic moment (produced by the electron, moving in an Bohr-like orbital around the nucleus). The efficiency of spin-orbit coupling, and therefore intersystem crossing, can usually be enhanced by the presence of heavy atoms.

Phosphorescence

Once the excited triplet state T_1 is reached it shows a relatively long lifetime compared to singlet states, which can reach time scales up to several seconds or even minutes. This is because all further de-excitation are being spin-forbidden. In solution at room temperature the radiative rate constant is very low and radiative de-excitation is unlikely due to frequent energy transfer to colliding solvent molecules. At these conditions non-radiative de-excitation is predominant. However, at low temperatures or by embedding in rigid matrices those collisions are reduced significantly and therefore phosphorescence can be observed.

Due to lower energy of the triplet state S_1 compared to the excited singlet state S_1, phosphorescence emission can be found at higher wavelengths than the respective fluorescence emission.

Reverse Intersystem Crossing and Delayed Fluorescence

Another possible pathway from the excited triplet state is reverse intersystem crossing from T_1 to S_1. *Thermally activated delayed fluorescence* (E-type) can occur if the energy difference between those electronic states is small and the lifetime of T_1 is long enough. The resulting fluorescence emission shows the same spectral properties as prompt fluorescence but shows lifetimes similar to phosphorescence (hence the name delayed fluorescence) because the molecules stays in the excited triplet state before emission form S_1. Since this transition is thermally activated and its efficiency increases with rising temperature.

Triplet-triplet annihilation (P-type) is another pathway that can happen in concentrated solutions. Here collision between two molecules in the excited triplet state can provide sufficient energy for one of them to return to the S_1 state. The resulting fluorescence emission is also delayed because of the electrons prior residence in the triplet state.

Table 2.1.: Characteristic times of electronic transitions.

Process	Time
Absorption	10^{-15} s
Vibrational relaxation	10^{-12}-10^{-10} s
Lifetime of excited state S_1	10^{-10}-10^{-7} s
Intersystem crossing	10^{-10}-10^{-8} s
Internal Conversion	10^{-11}-10^{-9} s
Lifetime of excited state T_1	10^{-6}-1 s

2.4.4. Lifetimes

Excited state lifetimes describe the time that a molecule stays in the excited state upon excitation until radiative- or non-radiative de-excitation occurs. The average lifetime of the excited state S_1 τ_s can be described as

$$\tau_s = \frac{1}{k_r^s + k_{nr}^s} \tag{2.13}$$

where 2.13 k_r^s and $k_n r^s$ denote the rate constant for radiative and non-radiative de-excitation from the S_1 state, respectively. The kinetics of the various de-excitation processes are generally of first order kinetics (except triplet-triplet annihilation)

$$[A^*] = [A^*]_0 \cdot e^{-\frac{t}{\tau}} \tag{2.14}$$

where 2.14 $[A^*]$ and $[A^*]_0$ describe the time evolution of the concentration of excited molecules at a certain time and the concentration of excited molecules at time 0, respectively. For organic molecules lifetimes of excited singlet states range from 10^{-11} to 10^{-7} s, while phosphorescence lifetimes are usually much longer and range from microseconds to seconds. However, this fact cannot be used to distinguish between fluorescence and phosphorescence because several inorganic compounds and organometallic compounds can show longer lifetimes. Determining the lifetime of a component can be experimentally done in the time and in the frequency domain (pulse- or phase-modulation fluorometry).

2.4.5. Quantum Yields

Quantum yields describes the fraction of excited molecules that by returning to the ground state emit photons. It can be described as the ratio between emitted and absorbed photons and

is an important parameter for sensor brightness. In the case of fluorescence the *fluorescence quantum yield* can be described as:

$$\Phi_F = \frac{\text{emitted photons}}{\text{absorbed photons}} = \frac{\tau_s}{\tau_r} = \frac{k_r}{k_r^s + k_{nr}^s} = k_r^s \cdot \tau_s \tag{2.15}$$

In general, it can be close to unity for fluorescence if the rate of radiative decay k_r^s is much higher than the rate of non-radiative decay k_{nr}^s. Quenching of excited molecules can lead to simultaneous decrease of quantum yields and lifetime of the excited state (dynamic quenching) or decreasing quantum yields without any change in excited state lifetime (static quenching).

To determine quantum yields of a unknown substance, usually a reference compound of known quantum yield (e.g. fluorescein, quinine sulfate, etc.) is used. The reference compound should match the spectrum of the sample to minimize errors, should not be susceptible to oxygen or concentration quenching and the measurement should be performed in similar conditions [55]. The quantum yield of the unknown substance can be calculated using

$$\Phi_F = \Phi_R \frac{I}{I_R} \frac{(1 - 10^{A_R})}{(1 - 10^{A})} \frac{n^2}{n_R^2} \tag{2.16}$$

where I is the integrated intensity, A is the absorbance and n is the refractive index. The subscript R denotes the reference sample. Furthermore, quantum yields and lifetime depend heavily on temperature. An increase in temperature favours non-radiative processes (intramolecular vibrations, rotations, collision with solvent molecules, etc.) and therefore decreases observed quantum yields. Other parameters like pH, polarity, viscosity, etc. can also affect quantum yields and lifetimes.

2.4.6. Intermolecular De-excitation Processes

All de-excitation processes presented above were of intrinsic nature. However, de-activation can also occur by interaction with a another molecule. *Quenching* describes the interaction of a quenching molecule (Q) with an excited (M^*) or non-excited molecule (M), resulting in the inhibition of photon emission. There are several possible photophysical processes that can result in fluorescence quenching like photoinduced electron transfer (PET), photoinduced proton transfer (PPT), collision with heavy atoms, energy transfer or the formation of excimers or exciplexes.

Dynamic Quenching describes the collision between the excited molecule and with quencher molecule like oxygen, acrylamide, succinimide, halides, etc. During collision energy is transferred non-radiatively from the excited molecule to the quencher causing the molecule to return to the

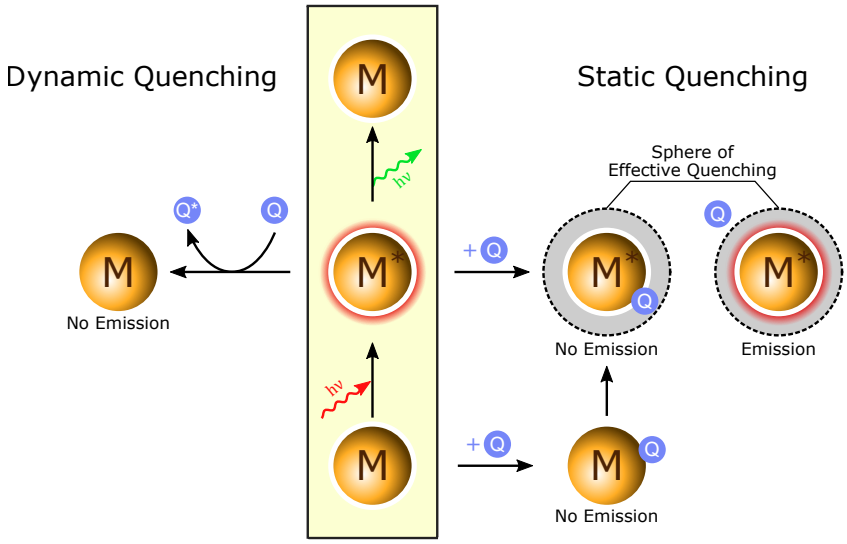

Figure 2.12.: Scheme of static and dynamic quenching.

ground state. The probability of collision is increased at higher lifetimes of the excited state. Dynamic quenching is a diffusion controlled process. Consequently, the quenching rate constant k_q is time dependent and both luminescence intensity and lifetime are affected. The decrease in luminescence quenching can be describe by the *Stern-Volmer equation*

$$\frac{I_0}{I} = \frac{\tau_0}{\tau} = \frac{\Phi_0}{\Phi} = 1 + k_q \tau_0 [Q] = 1 + K_{SV}[Q] \tag{2.17}$$

where I_0 and I are the steady-state fluorescence intensities in absence and presence of a quencher, respectively. $K_{SV} = k_q \tau_0$ is the Stern-Volmer constant and [Q] denotes the concentration of quencher molecules.

Static quenching takes place when the molecule and the quencher form a non-emitting complex. This can happen due to formation of a *ground-state non-luminescent complex*. Upon addition of a quencher the fluorescence intensity decreases, but the lifetime is unaffected. The decrease in fluorescence is dependent on the concentration of the quencher $[Q]$ and the stability constant of the formed complex K_S and can be described as

$$\frac{I_0}{I} = 1 + K_S[Q] \tag{2.18}$$

It can be possible to observe evidence of the formation of such complex (e.g. changes in absorption spectra), however this is not always possible. Therefore, another model was proposed by Perrin in which a *sphere of effective quenching* is introduced. This sphere has a certain

volume surrounding the fluorophore and if the quenching molecule is outside this sphere there is no interaction. Perrin's model can be described as

$$\frac{I_0}{I} = e^{(V_q N_a [Q])} \tag{2.19}$$

where V_q is the volume of the sphere of effective quenching and N_a denotes Avogadro's constant. Contrary to the previous presented quenching models (both show linear correlation of $\frac{I_0}{I} \propto [Q]$) this model shows an upward curvature at high quencher concentrations. However, at lower quencher concentrations the dependence is almost linear ($e^{V_q N_a [Q]} \approx 1 + V_q N_a [Q]$).

2.5. Chemical Sensors

Variations of optical phenomena of indicator dyes (e.g. fluorescence, phosphorescence or delayed fluorescence) can be used to sense various analytes. While these indicator dyes may be sensitive towards a certain analyte a complete sensor needs additional tools to facilitate excitation of the indicator and correct read-out in order to assess analyte concentrations. The following section describes the principle of chemical sensors and is based on references [51, 56–60]. All other sources will be referenced explicitly.

In general, a sensor is a small self-contained measurement device for a specific analyte. Its purpose is to detect changes or events in the environment and transduce this change to an electric signal that can be measured. IUPAC defines a chemical sensor as follows:

> "A chemical sensor is a device that transforms chemical information, ranging from the concentration of a specific sample component to total composition analysis, into an analytically useful signal. The chemical information, mentioned above, may originate from a chemical reaction of the analyte or from a physical property of the system investigated." [61]

An ideal sensor should fulfil certain requirements. It must be compact, robust, cheap, show high selectivity and sensitivity in a broad dynamic range and fast response times. Sensors usually consist of a *receptor* and a *transducer unit*. The receptor is the recognition element interacting with the sample and shows affinity for the analyte. This may be in the form of interactions like adsorption, ion exchange or a chemical reaction resulting in a change of one or more distinct properties or characteristics. The transducer unit then converts the chemical response signal of the receptor in a electric signal (e.g. current or voltage) that can be measured. The general stages in the operating procedure of a sensor are shown in Figure 2.13.

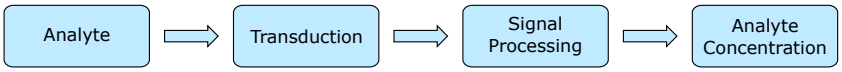

Figure 2.13.: Principle stages in the operation of a sensor.

Sensors can be classified by the transducer principle, the type of stimulus (electric, thermal, optical, etc.), the mode of application (in vivo/vitro), the method used for measuring the effect (e.g. catalytic devices) or according to the investigated analyte (e.g. oxygen sensors, pH sensors, etc.). The most common classification of sensors is the classification according to the operating principle of the transducer.

Optical sensors show a change in optical phenomena due to interaction of the analyte with the receptor. This comprises absorbance, luminescence, fluorescence, reflectance refractive index, optothermal and light scattering based sensors.

Electrochemical sensors transform the chemical information from the analyte - electrode interaction into a measurable signal. This includes voltammetric, potentiometric and field-effect transistor based sensors.

Electrical sensors are sensors where no electrochemical process takes place and the signal is solely acquired from the change of electrical properties due to interaction with the analyte (e.g. semiconductor sensors, electric permittivity sensors, etc.).

Mass sensitive sensors are based on the mass-change due to accumulation of analyte on a modified surface (e.g. piezoelectric sensors, surface acoustic wave sensors, etc.).

Magnetic sensors derive the signal due to the change of paramagnetic properties of the sample (e.g. oxygen).

Thermometric sensors measure heat effects of chemical reactions or adsorption due to interaction with the analyte.

Sensors based on other physical properties are based on different properties such as nuclear radiation.

2.5.1. Conventional pH Sensing Methods

pH Indicators and Indicator Paper

One of the simplest methods for pH determination are pH indicators or papers impregnated with pH indicators. Those compounds are halochromic substances which change colour upon protonation or deprotonation. To achieve a broader dynamic range usually various indicators

with different pK_a values are mixed. After submersion in the test solution the resulting colour is compared with a colour chart, which allows estimation of the sample's pH. Needless to say, this method is quite imprecise but due to its simplicity and low cost it is still widely used to get a rough estimation of a sample's pH.

Glass Electrode

Without a doubt, the most widely used measurement method for pH is the pH glass electrode. It is the most common ion selective electrode with a very broad dynamic range of 14 decades of H^+ concentration. It is a potentiometric measurement technique where the potential between the glass electrode and a reference electrode is measured.

Most commonly, combination electrodes comprise both external and internal reference electrode connected via a salt bridge in a single rod (Figure 2.14). Historically, Hg/Hg_2Cl_2 (saturated calomel electrode) was the most used reference electrode and it still offers the most constant reference potential up to date [62]. However, it has been mostly replaced by Ag/AgCl electrodes due to lower toxicity. The glass membrane is usually made from alkali-silicates, which forms a thin, water-swollen layer by exchanging alkali metal ions with protons from the surrounding medium.

$$\text{—SiO}^-\text{Na}^+ + \text{H}_3\text{O}^+ \rightleftharpoons \text{—SiO}^-\text{H}_3\text{O}^+ + \text{Na}^+_{(aq)}$$

The inside of the electrode is filled with a buffer solution (pH 7) containing KCl. Therefore, the proton concentration on the inside of the glass membrane is constant, while the concentration of protons on the outside depends on the pH of the sample solution. The resulting galvanic potential can be measured and described by the *Nernst equation*

$$E = E^0 + \frac{RT}{zF} ln \left(\frac{a_{ox}}{a_{red}} \right) \tag{2.20}$$

where E is the potential, E_0 is the standard potential, R is the gas constant, T is the temperature in Kelvin, z is the number of electrons involved in the electrochemical process, F is the Faraday constant and a_{ox} and a_{red} are the activities of the oxidized and reduced form, respectively. A typical assembly of a pH electrode can be described as:

$$\underbrace{\text{Ag/AgCl/KCl(sat.)}}_{\text{external reference electrode}} \text{ || test solution | } \underbrace{\text{glass membrane | } \underbrace{\text{internal buffer | } Ag/AgCl}_{\text{internal reference electrode}}}_{\text{glass electrode}}$$

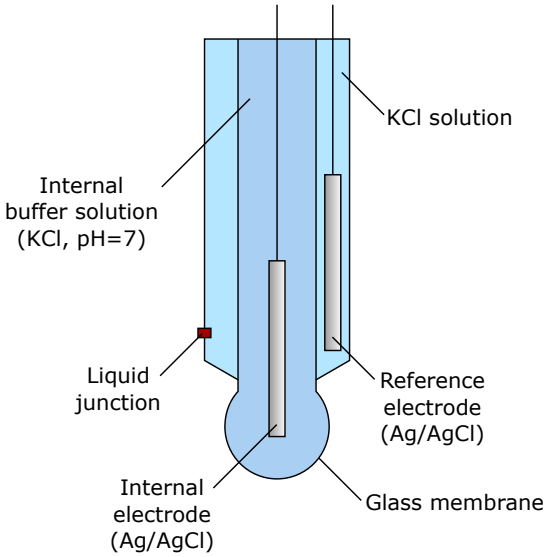

Figure 2.14.: Scheme of combination glass electrode.

The liquid junction || between the KCl solution and the sample solution provides the necessary electrical contact while minimizing flow of KCl into the the sample solution [63]. At this solution boundary a *liquid junction potential* arises. This potential is minimized by using saturated KCl solutions in an intermediate *salt bridge*. With increasing concentrations the ionic transport at the junction is dominated extensively by the vast amount of KCl, which consists of ions with nearly equal mobility [47]. By minimizing these potentials and since all other interfaces in the system feature phases of constant composition the remaining contribution from the sample solution is solely dependent on the potential difference across the glass membrane. This potential can be described by the *Nernst equation*:

$$E = E^0 + \frac{RT}{1 \cdot F} ln\ a_{H^+} \tag{2.21}$$

At ambient conditions (25 °C) the first part of this equation can be simplified to 59.16 mV, which corresponds to the typical slope of a pH electrode. However, owing to various effects like liquid junction potentials and deviations of the standard potential E^0, which is the sum of potential differences at all other interfaces, pH electrodes must be calibrated before use. This can be done by single-point, two-point and multi-point calibrations with standardized buffer solutions depending on the needed accuracy of the measurement [64].

While the pH electrode offers very robust measurement method over a broad pH range, it also has several limitations. Before measurement the glass membrane needs to be pre-conditioned for a certain time in order to swell the silicate framework. Also, for precise and reproducible measurement it requires frequent calibration. Furthermore, also other cations like Na^+ Li^+

and other mono-valent cations may penetrate the membrane and contribute to the measured potential. This is especially critical at very high pH values due to lack of hydrogen ions in the sample solution (*alkaline-error*).

2.5.2. Optical pH Sensors

Optical sensors are have gained popularity because they offer several distinct advantages in terms of sensitivity within their dynamic range, selectivity and response time. They enable remote sensing with optical fibres and even contactless measurements inside sealed containers is possible. Also they are not susceptible to electromagnetic interferences, need no external reference electrode and can be miniaturized with ease.

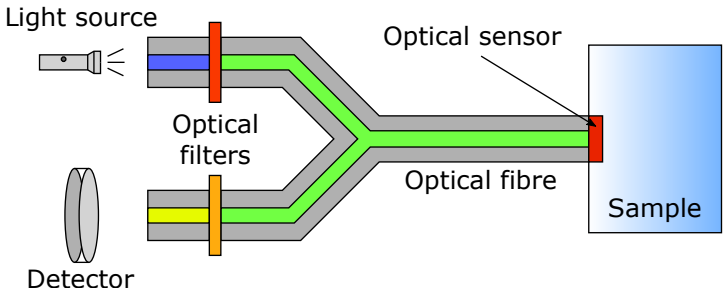

Figure 2.15.: Scheme of a fibre-optic sensor.

In general optical sensors follow the same principle as described above (Figure 2.13) as they comprise a transduction platform and a signal processing unit which transforms the chemical signal to yield the final analyte concentration. The main difference is that optical sensors are defined by the use of optical transduction techniques. The read-out (Figure 2.15) of the sensor also requires an excitation source (e.g. LED, tungsten-halogen lamps, etc.), optical filters, light guides to and from the sensitive material (e.g. optical fibres and planar waveguides) and a detector (e.g. photodiode, photomultiplier, etc.). A wide variety of optical sensors has been developed and their shapes and applications are manifold, ranging from fibre optic chemical sensors (FOCS) to planar waveguide-based chemical sensors (PWCS) and multianalyte array sensors.

Fluorescence-based pH sensors have two major components: a fluorescent pH probe and a immobilisation matrix. Usually the pH probe is a small organic molecule (i.e. fluorescent dye), fluorescent polymer or inorganic compound. In order to assess the pH of a sample, the pH probe needs to undergo a modulation of fluorescence phenomena (i.e. quantum yield, decay time or spectral shape). In contrast to potentiometric measurements, where the electrode's response is directly linked to the activity of the protons in solution, pH sensitive indicators show a change in the relative fraction of acid and base forms upon interaction with protons,

resulting in a change in photophysical properties. These changes can be detected by means of absorption or fluorescence measurements. The equilibrium between acidic (protonated) and basic (unprotonaed) form can be described by the *Henderson-Hasselbalch equation* (equation 2.2). The pH-sensitivity is highest at pH = pK_a but is generally limited to pH = $pK_a \pm 1.5$. Therefore, the choice of the appropriate indicator dye is crucial, since the sensitivity is given only in a narrow pH range. However, indicator dyes and can be easily tuned to fit a variety of pH regions [65] and can also be combined to cover a broad dynamic range [66].

The immobilisation matrix serves as thin-film environment where the pH sensitive material is homogeneously dispersed without aggregation. The matrix should provide high water uptake to ensure rapid equilibration of the sensor to the sample's pH. Most commonly, organic polymers and sol-gels are used. Entrapment of the indicator can be done either physically or by covalent coupling. Covalent linkage can increase the sensor's leaching-stability and minimize aggregation effects. However, both matrix and indicator often need further molecular modifications to facilitate covalent bonding. Choosing a suitable immobilisation matrix is crucial since it affects various properties of the final sensor probe like selectivity, response time, pK_a and stability.

Fluorescence intensity itself is a rather ambiguous parameter, since it is prone to fluctuations of the excitation light, indicator concentration, optical pathlength, photobleaching, aggregation, etc. To compensate for those effects and parameters which are not directly related to the analyte concentration a referencing method is required.

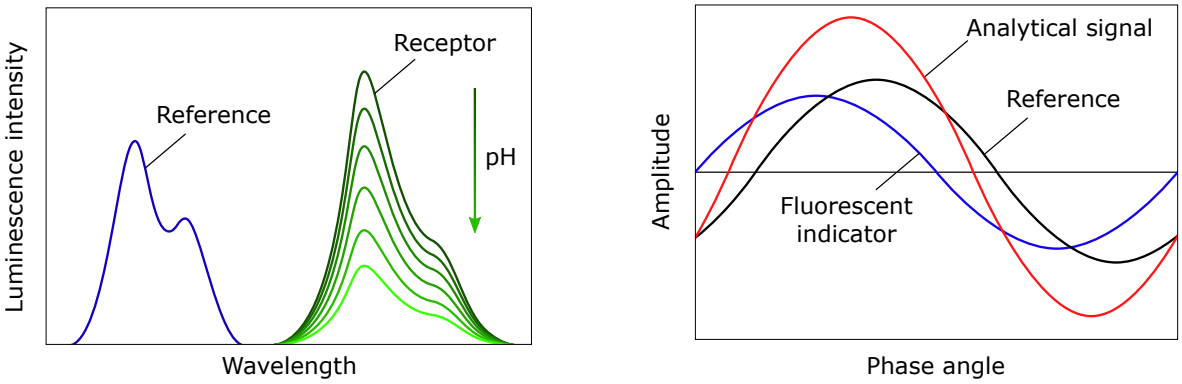

Figure 2.16.: Scheme of dual emission ratiometric referencing (left) and frequency domain dual-lifetime referencing (right)

Ratiometric referencing (Figure 2.16, left) is performed by evaluating the ratio of fluorescence intensities measured at two wavelengths. Therefore, it requires two spectrally distinguishable excitation or emission bands. Some probes offer a pH-dependent shift of the fluorescence spectrum and therefore do not need an additional reference fluorophore (self-referencing). However, since many dyes only emit at a single wavelength, a second dye excitable at the same wavelength and emitting at a different part of the spectrum can be added to the system for

referencing purposes. This external referencing dye must not be sensitive towards the analyte [67]. This procedure requires two separate optical channels, which can show different drifts in sensitivities and also the intensities at two excitation wavelengths can vary.

Because of that *decay time* and sometimes *anisotropy* are sometimes used instead of fluorescence intensity. Due their intrinsically referenced nature they are hardly affected by fluctuations of the fluorescence intensity. However, measurement of those parameters is much more complex and requires costly instrumentation, especially when using fluorophores with rather low decay times, which are commonly used in pH-sensors (nanosecond range).

Alternatively, referencing of the luminescence intensity can also be done by *dual lifetime referencing* (DLR) as can be seen in Figure 2.16 (right). This relies on the combination of the indicator with a pH-insensitive reference dye with significantly longer decay time. Both dyes are excited by the same modulated light source and the resulting phase-shift is depended on the luminescence intensity ratio between indicator and reference dye. This technique can be used in the frequency or time domain, but it has to be stated that DLR is not a true measurement of luminescence decay time but only a readout technique for fluorescence intensity based on phase-modulation fluorometry [68].

Part II.

Experimental

3. Materials and Methods

3.1. Methods

3.1.1. Absorption Spectra

Absorption spectra were aquired on a CLARIOstar Plus microplatereader from BMG Labtech (Ortenberg, Germany) in 96 well plates. Measurements were corrected by baseline measurement of pure solvent.

3.1.2. Cyclic Voltammetry

Cyclic Voltammetry (CV) measurements were performed using PalmSens4 from Palmsens (Houten, The Netherlands) or SPELEC from DropSens (Oviedo, Spain) in galvanostatic mode. The setup comprised three electrodes. The used electrodes can be seen in Table 3.3. Cyclic voltammogramms were recorded in the appropriate potential range for each combination of analyte, electrodes, electrolyte and solvent at different scan rates (10, 50, 100 and 500 mV/s).

3.1.3. Buffer preparation

Buffer solutions were prepared by dissolving appropriate amounts of buffer salts and electrolyte in deionized water (Milli-Q, 18 MΩ cm). HCl and NaOH standard solutions were used to adjust the pH to the desired value.

3.1.4. Optical pH Measurements

pH measurements were performed using a FireSting Pro multi-analyte meter, optical pH sensor probes and pH sensor spots, optical fibres, Pt100 temperature sensor for temperature compensation and buffers for calibration of the optical pH sensors (pH 4.01 and pH 10), obtained from Pyroscience (Aachen, Germany). The used sensors and equipment can be seen in table

3.2. The pH sensors were calibrated and used according to the user manual. Measurements were taken in a 5 s interval and signals were analysed using PyroWorkbench software.

3.2. Materials

Table 3.1.: Used Chemicals.

Chemical	Supplier
MOPS	Sigma-Aldrich
HEPES	Sigma-Aldrich
Sodium bicarbonate	Sigma-Aldrich
Sodium dithionite	Sigma-Aldrich
Sodium sulfate	Merck
Titrisol® (0.5 N HCl)	Merck
Hydrochloric acid	Merck
Sodium hydroxide	Merck
1,4-Benzoquinone	Sigma-Aldrich
Anthraquinone-2,7-disulfonic acid disodium salt	BOC Sciences

Table 3.2.: Optical sensors, meters and accessories.

Optical sensors and equipment	Supplier
pH6-8 sensor spot (PHSP5-PK7)	Pyroscience
pH7-9 sensor spot (PHSP5-PK8)	Pyroscience
pH6-8 sensor probe (PHROB-PK7)	Pyroscience
pH7-9 sensor probe (PHROB-PK8)	Pyroscience
Bare optical fibre (SPFIB)	Pyroscience
FireSting pro (FSPRO-4)	Pyroscience
Microplatereader (CLARIOstar Plus)	BMG Labtech

Table 3.3.: Electrodes, electrochemistry and spectroelectrochemistry equipment.

Electrodes and equipment	Supplier
Potentiostat/Galvanostat (PalmSens4)	PalmSens
Bipotentiostat/Galvanostat and Spectrometer (SPELEC)	DropSens
Screen printed carbon electrodes, Aux.: C; Ref.: Ag (ItalSens IS-C)	PalmSens
Screen printed gold electrodes, Aux.: Au; Ref.: Ag	Metrohm

Table 3.4.: Other chemicals, materials and devices used.

Other chemicals and materials	Supplier
UV curing glue (Loctite 3494)	Henkel-Adhesives
Silicone glue (Elastosil E43)	Wacker
Glass slides	Hounisen
Syringe filter (Chromafil GF/PET-20/25)	Machery-Nagel
pH meter (SevenCompact)	Mettler Toledo
pH electrode (InLab Science Pro-ISM)	Metler Toledo
pH microelectrode	In-house production
Digital buret (775 Dosimat)	Metrohm
pH meter (744 pH meter)	Metrohm
Peristaltic pump (502s)	Watson-Marlow

4. Experimental Procedure

4.1. Buffer Capacity Measurement

4.1.1. Cell Fabrication

The measuring flow-cell was fabricated according to Figure 2. Exact measurements can be seen in Figure A.1 in the appendix. While the glass slides and electrodes were glued with UV-curing glue, the pH sensors spots were attached to the glass with transparent silicone glue. This ensured that no light from the indicator dye got absorbed by the glue. A three electrode setup (working electrode = carbon, counter electrode = carbon, quasireference electrode = silver) was established inside the channel. Working and counter electrode were separated by approx. 5 cm in order to prevent mixing of the compartments directly over the electrodes. The quasireference electrode was positioned in between working and auxiliary electrode, with approx. 2.5 cm distance to the other electrodes.

Several different setups (open cell single sensor, open cell dual sensor, open cell pH optical and electrode measurement, dipping probe, closed flow cell) were produced similar to the fabrication presented below and are discussed in detail in the results and discussion section.

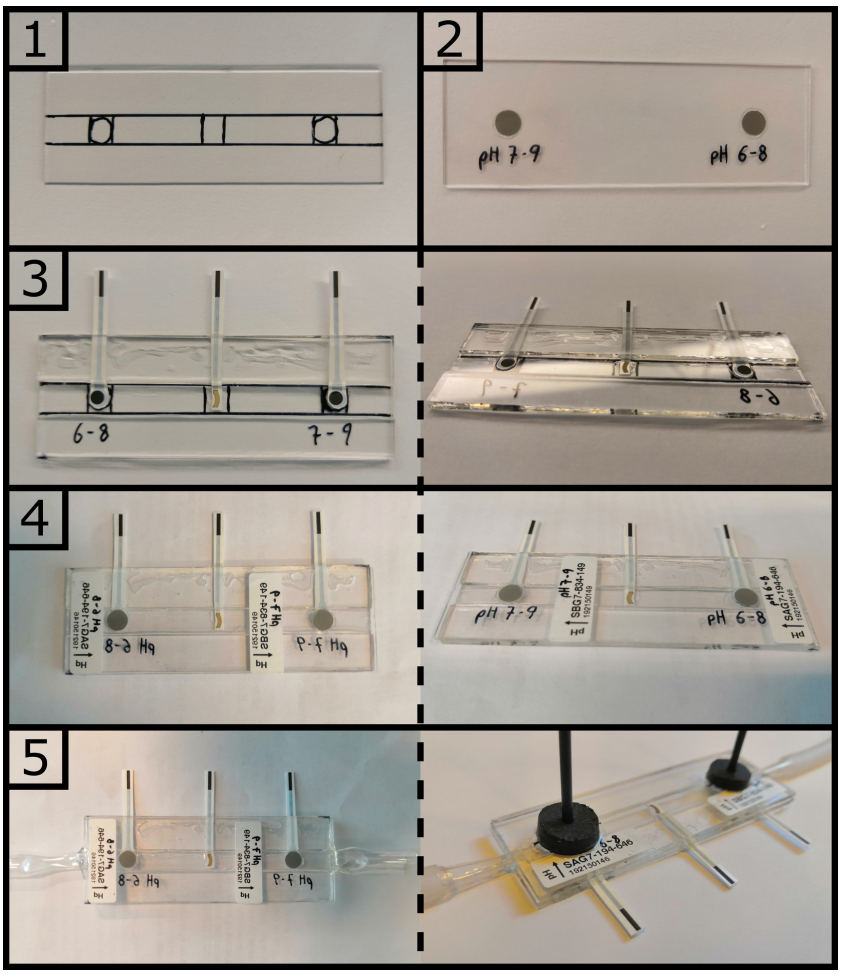

Figure 4.1.: Fabrication of measurement cell. 1) Layout of cell. 2) Fixation of sensor spots with silicone glue. The glue was left to cure overnight. 3) Screen printed electrodes were cut and glued onto a glass slide using UV-curing glue. Two smaller glass pieces were glued on top of the electrodes forming a channel. 4) The glass slide bearing the sensor spots was glued on top to close the channel. 5) In- and outlet adapters (PE), tubing (silicone) and adaptors for optical fibres (NR) were attached to the cell.

4.1.2. Measurement Setup

The three electrodes of the measurement cell were connected to a potentiostat and optical fibres were used to connect the cell to the optical pH meter. A peristaltic pump was used to introduce sample solutions into the measurement cell at a constant rate.

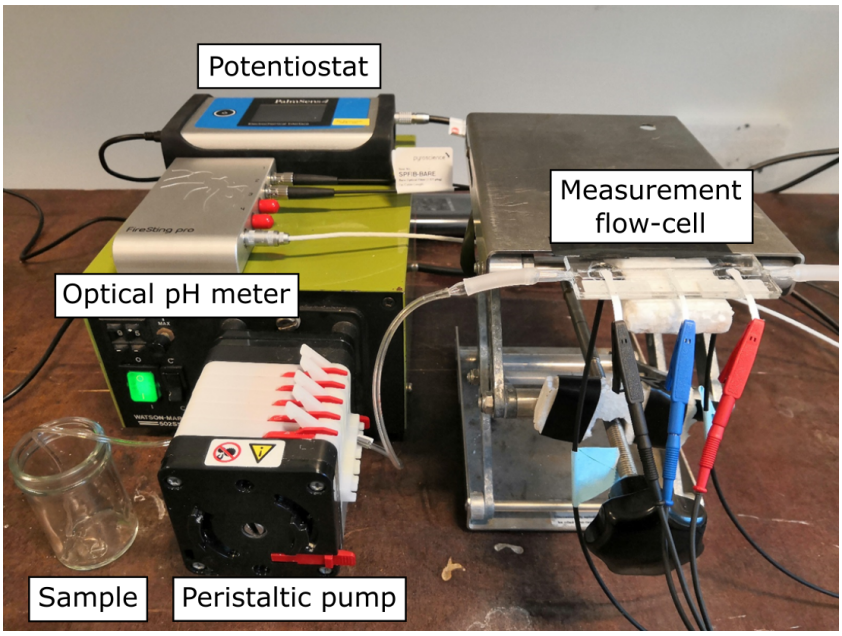

Figure 4.2.: Setup for buffer capacity measurement.

4.1.3. Sample Preparation

Surface water was taken from a lake in Vennelystparken, Aarhus, Denmark (56°09'53.7"N, 10°12'28.7"E). Sediment was retrieved from the same lake. The samples were centrifuged at 2500 rpm for 10 min and filtered using a syringe filter (pore size: 0.2 μm). Sodium sulfate salt was dissolved in the sample solutions to reach a final concentration of 0.5 M.

4.1.4. Calibration and Measurement

Several calibrations using different buffer salts were carried out at room temperature (21 °C). MOPS and HEPES calibrations were performed at buffer concentrations 2, 5, 10, 15, 20, 30, 50 and 100 mM. Bicarbonate calibration was performed at buffer concentrations 2, 3.5, 5, 7.5, 10, 15, 20 and 30 mM. MOPS buffer was measured at three different pH values (6.2, 7.2 and 8.2). HEPES and bicarbonate buffer were measured at pH 7.55 and 8.4, respectively. Additionally, solutions of 20 mM MOPS buffer were measured at pH 6.9, 7.2, 7.5, 7.8 and 8.2 to determine

the apparent pK_a at given temperature and ionic strength. To all buffer and sample solutions 0.5 M Na_2SO_4 was added as supporting electrolyte.

Measurements were performed by flushing the cell with buffer or sample solution (12 mL min^{-1} flow rate) until a stable baseline pH was observed. To ensure stagnant conditions the system was left without flow for at least 10 s prior to starting the measurement. After that a potential pulse (-2 V, 10 s) was applied and the change in pH near the electrodes recorded. The two sensors were read out with a phase-fluorometric four-channel FireSting pro device.

4.2. Titrations

For accurate titrations a digital buret in combination with a pH electrode from Metrohm (Herisau, Switzerland) was used. The pH electrode was two-point calibrated in the appropriate pH range using commercial available buffer solutions.

4.2.1. pK_a Determination of MOPS Buffer

The pK_a of MOPS was evaluated by titrating a solution of 20 mM MOPS buffer and 0.5 M Na_2SO_4, adjusted to pH 10.5 with NaOH, with 0.1 N HCl until a pH value of 4 was reached (20 mL sample volume). The titrant was added in 50 μL increments and the pH was recorded after each increment as soon as it was stable. The titration was performed at 24 °C under constant stirring and the headspace was flushed with nitrogen.

4.2.2. Total Alkalinity

Total alkalinity of the MOPS buffer calibration series (2, 5, 10, 15, 20, 30, 50 and 100 mM) and the lake surface and pore water samples was evaluated by end-point titration of the samples (20 mL sample volume) with 0.1 N HCl to pH 4.5. All samples were titrated with a 0.5 M Na_2SO_4 background to mimic the measuring conditions of the proposed measuring system mentioned in section 4.1. The titrations were performed at 24 °C under constant stirring and the headspace was flushed with nitrogen.

4.3. Characterization of Quinones

4.3.1. Cyclic Voltammetry Studies

Two quinones, 1,4-benzoquinone (BQ) and anthraquinone-2,7-disulfonic acid (AQDS) were characterized by cyclic voltammetry using a standard three-electrode configuration (screen-printed gold or screen-printed carbon, as can be seen in Table 3.3). A background CV was recorded before each CV experiment to exclude background contaminations. For each quinone a new set of electrodes was used.

Since the used AQDS was not pure (approx. 80 %, impurities: mostly carbonates), it was treated with 0.1 M HCl in order to convert the carbonates to carbon dioxide. After removal of the carbonates the pH was adjusted back to the initial value (approx. pH 7).

4.3.2. CV Analysis

The electrochemical reversibility was assessed by recording cyclic voltammogramms of each quinone. Each CV was analysed in terms of peak potentials and peak currents. A plot of peak currents to the square root of the scan rate was created and, if applicable, a linear fit performed to evaluate the electrochemical (Nernstian) reversibility of the electron-transfer reactions.

Furthermore, the electrochemical stability was evaluated by recording 10 cycles of cyclic voltammetry and comparing peak currents throughout the experiment.

4.3.3. Spectrophotometric Determination of the pK_a of AQDS

To determine the pK_a 1 mM AQDS solutions in 10 mM phosphate buffer with different pH values (6, 6.5, 7, 7.5, 8, 9 and 10), in 10 mM NaOH and 10 mM HCl were prepared. The sample solutions were transferred into a 96 well plate and read out with a CLARIOstar Plus microplatereader. All measurements were baseline corrected by subtracting the absorption spectrum of the pure solvent.

Part III.

Results and Discussion

5. Buffer Capacity Measurement

5.1. Measuring Principle

Buffer capacity is the resistance of a buffer solution to withstand pH changes upon addition of acid or base. Conventionally total alkalinity and total acidity is measured by volumetric titration with a acid with known concentration. However, this stepwise addition of strong acids while recording the pH is time-consuming and also requires standardized titrants [69, 70].

The proposed system uses water electrolysis to produce acid or base in-situ at the electrodes, as can be seen in equation 5.1. Therefore, no external titrant has to be introduced to the system and the amount of acid and base produced can be controlled by regulating the applied potential and pulse time. Depending on the applied potential the pH can be increased or decreased close to the working electrode (WE). The opposite effect is observed at the counter electrode (CE).

$$\begin{aligned} Anode(oxidation): \quad & H_2O(l) \quad \rightleftharpoons \quad 2H^+(aq) \; + \; \tfrac{1}{2}O_2(g) \; + \; 2e^- \\ Cathode(reduction): \quad & 2H_2O(l) \; + \; 2e^- \quad \rightleftharpoons \quad 2OH^-(aq) \; + \; H_2(g) \\ \hline Overall: \quad & H_2O(l) \quad \rightleftharpoons \quad \tfrac{1}{2}O_2(g) \; + \; H_2(g) \end{aligned} \tag{5.1}$$

The general measuring principle is depicted in Figure 5.1. The measurement cell is flushed with sample and the system is left without flow to ensure stagnant conditions and a stable pH reading. Water electrolysis is then induced by applying a potential pulse to the electrodes for a certain amount of time. Depending on the buffer concentration in the sample the buffer counteracts this pH change and therefore smaller peaks are recorded with increasing buffer concentration.

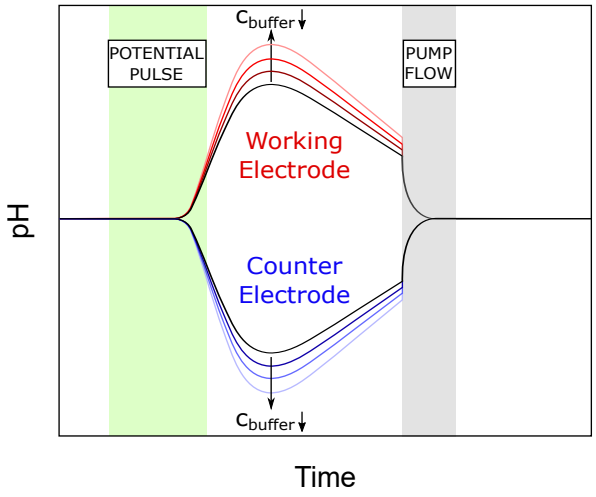

Figure 5.1.: Scheme for buffer capacity measurement.

5.2. Key Parameters

Electrode Materials

In general there is a wide variety of possible electrodes available to perform water electrolysis. The electrodes should preferably be made from a material with high conductivity, resistance to corrosion and erosion during the water splitting process and high catalytic activity for the hydrogen evolution reaction (HER) and the oxygen evolution reaction (OER). For industrial use another factor is price, making non-precious materials more attractive. Materials like stainless steel and nickel for cathodic materials and titanium coated with oxides and mixed oxides of metals like nickel and cobalt for anodic materials can generally be used. However they are quite unstable and susceptible to corrosion at low to neutral pH and are usually only used in alkaline water electrolysis. In addition to altering the electrochemistry this instability may also lead to contamination of the sample solution [71].

However, since in this system energy efficiency is not the limiting factor, the main criteria for the choice of material is stability. Therefore, carbon electrodes were used, since carbon meets the necessary requirements for this usage: it is electrically conductive, electrochemically, chemically (especially at negative potential regions [72]) and thermally stable [73]. One possible side reaction is the corrosion of the carbon electrode to form CO_2 by anodic oxidation, especially with increasing pH (Equation 5.2). This effect is mainly observed in industrial chlor-alkali processes performed at low pH and might translate to water electrolysis in this system. While slightly reducing the amount of active area of the carbon electrode, the amount of protons

generated and therefore the pH shift stays the same compared to water electrolysis [74].

$$C + 2H_2O - 4e^- \rightarrow CO_2 + 4H^+ \tag{5.2}$$

In general, platinum or more sophistacated materials would be more suitable because they offer lower overpotentials for water electrolysis. However, electrochemical performance is not the main criteria for the proposed setup. Therefore, any electrode meeting the necessary stability requirement and offer the possibility of miniaturization in the form of screen printed or sputtered electrodes will work.

The reference electrode material of choice was a Ag/Ag^+ quasi reference electrode. The main reason for this is the ease of miniaturization, which is necessary to fit into a small flow channel. If a regular reference electrode, e.g. Ag/AgCl, was used it would need to be isolated from the bulk solution with a glass frit or salt bridge. Furthermore, there is no liquid junction potential observable and usually there is no contamination of the sample solution by solvent molecules or ions which a conventional reference electrode might transfer [75].

Separation of Electrodes

The application of a certain potential pulse leads to a local change in pH close to the working and counter electrode. Application of a negative potential (-2 V vs. Ag/Ag^+) leads to an increase of pH close to the working electrode and a decrease of pH close to the counter electrode. By reversing the potential, i.e. +2 V vs. Ag/Ag^+, the opposite effect is observed. Therefore, the separation of those electrodes is crucial in order to avoid mixing of the two compartments. Figure 5.2 illustrates this pH change by using AQDS and BQ as pH sensitive indicator dyes. At high pH the quinone solutions turn dark red, almost black, while at low pH they show yellow (AQDS) and light orange (BQ) colour.

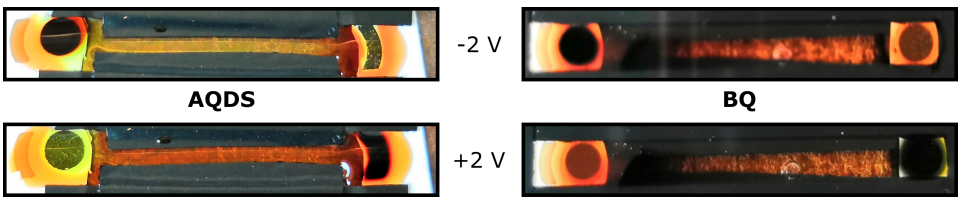

Figure 5.2.: Local change in pH close to working and counter electrode by application of ± 2 V pulses for 10 s. AQDS and BQ were used as indicator dyes in aqueous solution. Displayed potential differences are given vs. Ag/Ag^+ pseudoreference electrode.

Supporting Electrolyte

Pure water conducts an electric current very poorly and, for this reason, it is difficult to perform electrochemistry in it. Therefore, salts are added to increase conductivity to drive electrolysis at a significant rate.

Water electrolysis experiments were performed in 0.5 M NaCl, KCl or Na_2SO_4. Both NaCl and KCl contain chloride anions, which may undergo redox reactions on the electrode during application of a potential pulse. Equations 5.3 and 5.4 show the oxygen evolution reaction (OER) and chlorine evolution reaction (CER) in acidic media with their corresponding standard equilibrium potentials [76]. While the standard potentials for the used system are certainly different from the potentials needed using a Ag/Ag^+ reference electrode, it still shows that the required potentials are quite similar for both reactions. By application of a potential which is not exactly the potential needed to split water but slightly higher, the oxidation of chloride ions to gaseous chlorine is a competitive reaction. The exchange current density of CER was reported about 3-7 orders of magnitude higher than OER [77] due to a easier catalysed two-electron process compared to the four-electron process of water electrolysis [78].

$$\begin{aligned} 2H_2O &\rightleftharpoons O_2 + 4H^+ + 4e^- \\ E^0_{O_2/H_2O} &= 1.229\ V\ vs.\ RHE \end{aligned} \tag{5.3}$$

$$\begin{aligned} 2Cl^- &\rightleftharpoons Cl_2 + 2e^- \\ E^0_{Cl_2/Cl^-} &= 1.358\ V\ vs.\ RHE \end{aligned} \tag{5.4}$$

At higher pH the formation of hypchlorous acid or hypochlorite becomes thermodynamically favoured. Chlorine generated at the anode is immediately hydrolysed, which also generates H^+ as described in equation 5.5. Thus, with increasing pH the direct electrochemical formation of hypochlorous acid or hypochlorite is thermodynamically favoured compared to CER. This means that also during the chloride reduction the pH changes. However, the amount of pH change due to OER and CER is not the same.

$$\begin{aligned} Cl_2 + H_2O &\rightleftharpoons HClO + Cl^- + H^+ \\ HClO &\rightleftharpoons ClO^- + H^+ \end{aligned} \tag{5.5}$$

In dilute buffer solutions the pH changes very drastic at the electrode surfaces. The acidification of the environment around the anode during electrolysis leads to predominance of CER [79].

This means even if in the beginning of the potential pulse mainly oxygen is formed, the ratio of OER to CER will change with pulse time due to continuous acidification of the medium at the anode. Another negative effect of chlorine evolution is the highly corrosive nature of chlorine gas and chloride ions. Graphite electrodes have been shown to be susceptible to corrosion during brine electrolysis, due to nucleophilic attack of water and the formation of a chloride-graphite compound. This compound subsequently decomposes to carbon slime, carbon monoxide, carbon dioxide, chlorine gases and water [80].

All these effects lead to the conclusion that chlorine containing electrolytes are not the best choice for water electrolysis for controlled local alteration of pH. However, by finely tuning the applied potential in the measuring cell most side electrochemical reactions with only slightly higher overpotentials like CER can be avoided to great extent. Thus, even samples containing high Cl^- concentrations like seawater or other physiological samples can be measured [81]. To avoid any chloride production during investigation of various different setups (this would require fine-tuning each individual cell if chloride containing electrolytes were used) Na_2SO_4 was used as electrolyte instead. Both ions, Na^+ and ${SO_4}^{2-}$ are stable in the used conditions and do not show electrochemical conversion at the electrodes at the used potential ranges. The standard electrode potentials for both ions are shown in equation 5.6 and 5.7 [82].

$$\begin{aligned} &Na^+ + e^- \quad \rightleftharpoons \quad Na(s) \\ &E^0 = -\,2.71\ V\ vs.\ RHE \end{aligned} \tag{5.6}$$

$$\begin{aligned} &S_2O_8^{2-} + 2e^- \quad \rightleftharpoons \quad 2SO_4^{2-} \\ &E^0 = +\,2.01\ V\ vs.\ RHE \end{aligned} \tag{5.7}$$

Figure 5.3 shows the cyclic voltammograms of 2 and 100 mM MOPS buffer in 0.5 M NaCl and Na_2SO_4. While both show similar electrochemical windows a new redox peak pair at around 0.8 V is observed in the cyclic voltammogram of the MOPS/NaCl solution. This peak seems to undergo quasi-reversible electron transfer reaction at moderate to high buffer concentrations, while being irreversible at very low buffer concentrations.

Potential and Pulse Time

Choosing the right potential and pulse time are crucial parameters to generate reproducible results. The potential needed for water electrolysis depends on various parameters: electrode materials, distance between electrodes, type of electrolyte and electrolyte concentration. By

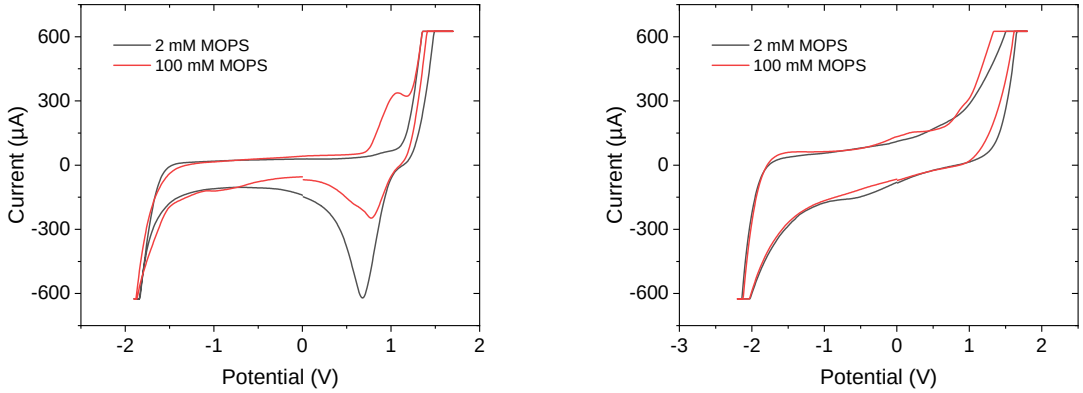

Figure 5.3.: Cyclic voltammograms of 2 and 100 mM MOPS (pH 7.2) in 0.5 M NaCl (left) and Na_2SO_4 (right) recorded at 10 mV/s.

changing those parameters, variations in the system's ohmic resistance are observed and a certain overpotential is needed to drive the reaction.

By recording cyclic voltammograms of buffer solutions at various concentrations with a constant electrolyte concentration in the measuring setup the minimal potential needed for water electrolysis was investigated. By choosing only the lowest possible potential to drive the reaction other undesired reactions which might occur at higher potentials can be prevented. Furthermore, lower applied potential also decreases the reaction rate which reduces bubble formation during the pulse time. This is especially crucial in the cathodic compartment where H_2 is produced because according to equation 5.1 for each two electrons transferred double the amount of hydrogen is produced compared to the oxygen production at the anode. In combination with the fact that the solubility of H_2 in water ($x_{H_2} = 1\ .411 \times 10^{-5}$ [83]) is lower than the solubility of O_2 in water ($x_{O_2} = 2.293 \times 10^{-5}$ [84]), the probability of bubble formation is substantially higher at the cathode.

5.3. Setup Ideas

5.3.1. Single Optical pH Sensor Cell

At first a single pH sensor probe was implemented into the measuring cell, as can be seen in Figure 5.4. To minimize interference with produced bubbles with the sensor, the sensor probe was introduced at a 90 ° angle. The sample was introduced into the channel using a syringe. After each measurement the sample solution was removed from the cell, the cell was rinsed with deionized water and a new sample solution was introduced.

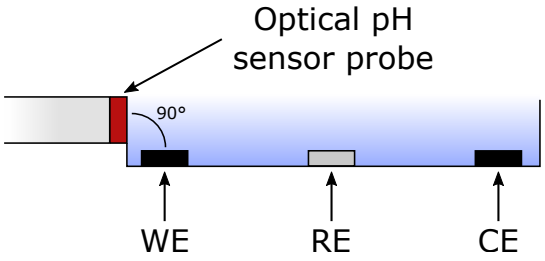

Figure 5.4.: Scheme of single sensor measuring cell.

In this setup only the pH close to the working electrode was monitored. Depending on the desired change in pH either a positive or a negative potential was applied. Figure 5.5 exemplifies this principle by application of ±3 V pulses for 5 s to a MOPS/Na_2SO_4 sample solution.

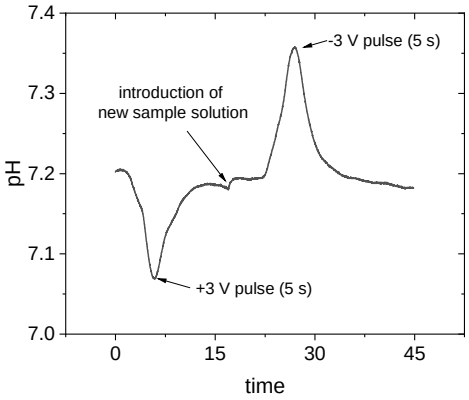

Figure 5.5.: pH readings close to the working electrode during application of 5 s +3 V and -3 V pulses applied to a solution of 2 mM MOPS and 0.5 M Na_2SO_4 in a open, single optical pH sensor cell.

Due to a single optical pH sensor this system is limited to a quite narrow pH range depending on the pK_a of the used indicator dye. In this case a sensor for a pH range of 7-9 was used. This allowed the investigation of buffer capacity of samples with near neutral pH by application of negative potentials in order to increase the pH close to the sensor.

5.3.2. Dual Optical pH Sensor Approach

By application of a second optical pH sensor close to the counter electrode both pH increase and decrease can be monitored. Figure 5.6 shows the schematics of the setup. Furthermore, the introduction of a second sensor with different pK_a facilitates an increase in effective pH range of the system. In this case a pH 7-9 sensor was installed close to the working electrode and

a pH 6-8 sensor was deployed close to the counter electrode. Therefore, pH changes in both directions from the neutral pH sample can be monitored.

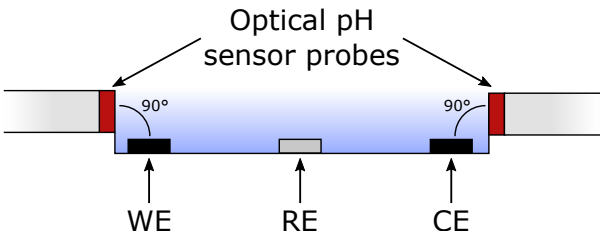

Figure 5.6.: Scheme of dual sensor measuring cell.

Figure 5.7 shows the simultaneous measurement of pH close to both electrodes. It also shows quite big inconsistencies in the recorded signal throughout several equal pulses. Due to the open nature of the measurement cell it is very susceptible to external influences introducing flow to the sample and also evaporation of the sample solution. Any introduced flow to the system influences the signal and results in uneven curves.

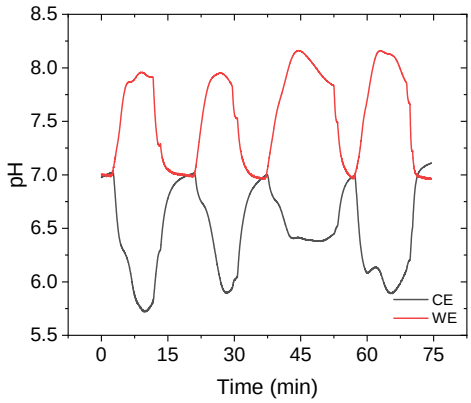

Figure 5.7.: pH readings near anodic and cathodic compartment during several 10 s -2 V pulses applied to a solution of 5 mM MOPS and 0.5 M Na_2SO_4 in a open dual optical pH sensor cell.

5.3.3. Comparison to pH Microelectrode

For comparison a pH microelectrode was installed only a few micrometers from the electrode, as shown in Figure 5.8. Due to the fragility of the used microsensor it was installed in an open measuring cell. Furthermore, when using a pH electrode it is necessary to use it in combination with an appropriate reference electrode. Therefore, a Ag/AgCl reference electrode was introduced between counter and reference electrode of the water electrolysis setup.

Figure 5.9 shows the pH signals of both sensors. Noticeably, the response time for the pH

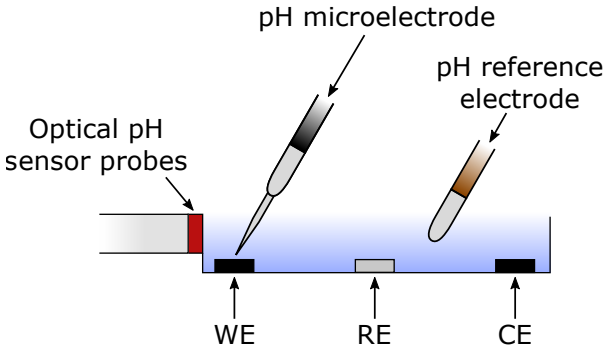

Figure 5.8.: Scheme simultaneous measurement of pH with optical sensor and microelectrode.

microelectrode is much lower because it is closer to the electrode where the pH change occurs. However it also seems to be more susceptible to flow being introduced to the system. This flow can be introduced externally due to the open measuring cell or in smaller scale by the formation of bubbles at high applied voltage and extended pulse times. Even if not visible to the eye nano- and microbubbles may be generated due to electrolysis at both electrodes [85, 86].

Furthermore, the pH electrode shows severe electromagnetic interferences during application of the potential pulse. In figure 5.9 a drastic pH increase to pH 14 and above is recorded by the pH microelectrode right as the potential pulse is applied. Immediately after the pulse the recorded pH value drops back to baseline.

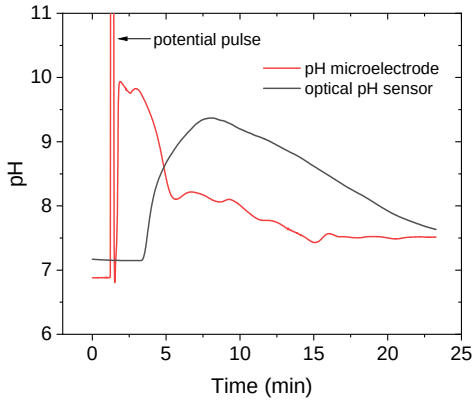

Figure 5.9.: pH readings of optical pH sensor and pH microelectrode during application of -3 V pulse for 10 s to a solution of 2 mM MOPS and 0.5 M Na_2SO_4.

5.3.4. Dipping Probe

Another investigated setup was the dipping probe. The schematics of this setup are illustrated in Figure 5.10. While the working electrode was installed as close to the sensor as possible,

the counter electrode was positioned further away on the steel casing of the pH probe to avoid mixing of the two compartments. It allows easy submersion of the sensing system in the sample solution and portability. However, since there is some distance between working electrode and the pH sensor, the system relies on diffusion of the generated acid or base to the sensor. In order to generate reproducible results, the sensing system must be completely motionless, i.e. it can not be hand-held and there also should not be any motion in the sample solution itself. This ensures there is no convection in the sample solution and any recorded pH change is purely related to the diffusion of generated acid or base from the electrode.

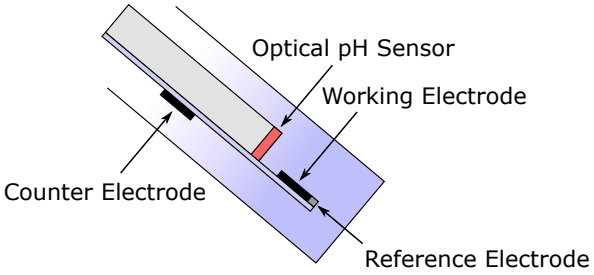

Figure 5.10.: Scheme of dipping probe setup.

5.3.5. Closed Flow Cell

The main problem with open-cell systems like the systems mentioned above is that the sample solution is exposed to ambient air at the liquid-air interface during measurement. Since water has substantial vapour pressure at ambient conditions it is constantly evaporating at the sample surface [82]. This leads to concentration gradients of the dissolved salts and buffering agents, which might induce diffusion in the sample solution. Furthermore, exposure to air can lead to exchange of CO_2 with the overlaying air. This can alter the initial pH of the sample solution as well as the buffer capacity (mainly when carbonate buffer species are present in the sample). These effects are even more pronounced when very small sample volumes are used.

Therefore, a completely closed flow system was built, as can be seen in Figure 5.11. Optical sensors are used instead of potentiometric sensors because they are not susceptible to electromagnetic interferences and allow contactless measurement and therefore are able to measure in a fully closed cell. Sample solution is introduced via a peristaltic pump and then the cell is closed of via two valves right before and after the electrodes and sensor spots. This ensures no flow is present in the system, eliminating the effects presented above. To minimize the effect of generated bubbles on the optical sensors, the electrodes are positioned above the sensors. This ensures that if bubbles were to be generated they would stay at the electrode surface, separated from the sensors.

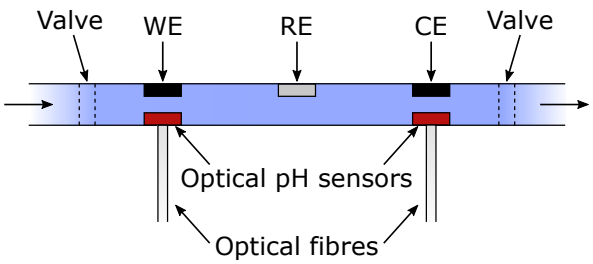

Figure 5.11.: Scheme of closed flow cell.

5.4. Data Evaluation

Different approaches were investigated to evaluate the obtained raw data. Figure 5.12 illustrates the two main methods investigated. The first method (blue) uses absolute pH values. ΔpH is calculated by subtracting the baseline pH from the peak pH. While this method gives accurate results it is quite time consuming, because depending on the buffer concentration it can take up to 5 min to reach the pH peak of the measurement.

Therefore, a different approach was investigated. Instead of absolute pH values the maximum rate of pH change (maximum slope) is monitored. This non-equilibrium read-out allows to substantially reduce the measuring time because it is not required to reach the pH peak of each measurement and the cell can already be flushed with new sample solution. Furthermore, this allows to calibrate for a broader range of buffer concentrations. At a constant applied potential and pulse time, e.g. -2 V for 10 s, low buffer concentrations lead to a very big pH increase at the one electrode and a decrease at the other. Consequently peak pH values are going to be shifted further from the initial pH of the sample solution and at a certain threshold the peak pH values are not within the dynamic range of the optical pH sensors any more. Since the maximum slope is usually found at approx. half of the peak height, this methods allows to investigate a broader range of buffer concentrations.

The obtained raw data of a MOPS calibration series (at pH = pK_a = 7.2) measured in triplicates with a dual sensor closed flow cell is shown in Figure 5.13 (left). MOPS buffer was used as it is stable in the used potential range. While small amounts of oxidation can be achieved chemically with H_2O_2 (only negligible amounts in a short time frame) [87], no redox activity of MOPS was observed using common electrochemical methods [88, 89]. The first derivative is formed to obtain the rate of pH change per time interval (right). The peaks correspond to the maximum rate of pH change for each measurement. Here the evaluation is only shown for the working electrode compartment. The evaluation of the counter reaction can be done according to the same principle.

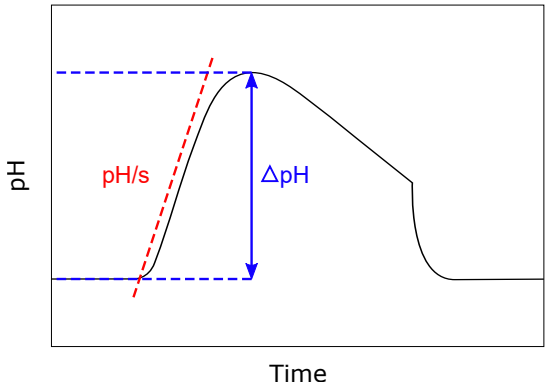

Figure 5.12.: Scheme for the evaluation of obtained raw data using ΔpH of each peak (blue) and using the slope and therefore the rate of pH change (red).

Figure 5.13 also shows different magnitudes of pH change for the two electrode compartments. In general similar peak heights in both directions are expected since for every electron transferred the same amount of protons and hydroxyl ions are produced. Small differences are expected due to higher mobility of H^+ compared to OH^- [90]. However, the main reason for different magnitudes of pH change is most likely related to slight differences in geometry of the measuring cell. Minor differences in the distance between pH sensor and electrode due to manual fabrication of the measuring cell lead to different diffusion lengths from the origin of pH change to the sensor in both compartments.

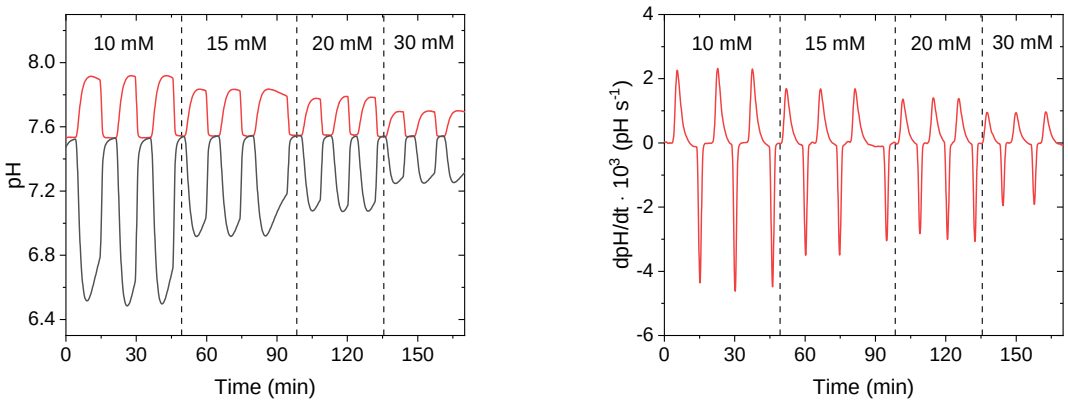

Figure 5.13.: pH readings close to working (red) and counter electrode (black) for different concentrations of MOPS buffer measured in triplicates (left) and rate of pH change in the working electrode compartment (right).

5.5. Dependence on Electrolyte Concentration

In general the conductivity of an electrolyte depends on (i) the concentration of free charge carries (ions) in solution and (ii) the mobility of those ions in an electric field. At high salt concentrations a lot of charge carriers are present and more concentrated solutions are expected to exhibit higher conductivities and promote higher reaction rates at the electrodes at a certain potential. This expectation only fails at very high salt concentrations close to the solubility limit due to lack of solvent molecules [48].

All conducted experiments were performed with using Na_2SO_4 as electrolyte. Figure 5.14 shows the pH change rates of 20 mM MOPS buffer with increasing electrolyte concentrations. A linear increase at the working electrode and a linear decrease at the counter electrode are observed by application of negative potential pulses. Small deviations can be seen at very low and very high electrolyte concentrations. At low concentrations the reaction rate and therefore the pH change is very small due to the lack of charge carriers in solution. At very high concentrations small deviations are observed due to reaching the solubility limit of sodium sulfate in water (1.12 M in water at 20 °C [91]). Therefore, a concentration of 0.5 M Na_2SO_4 was used for further experiments.

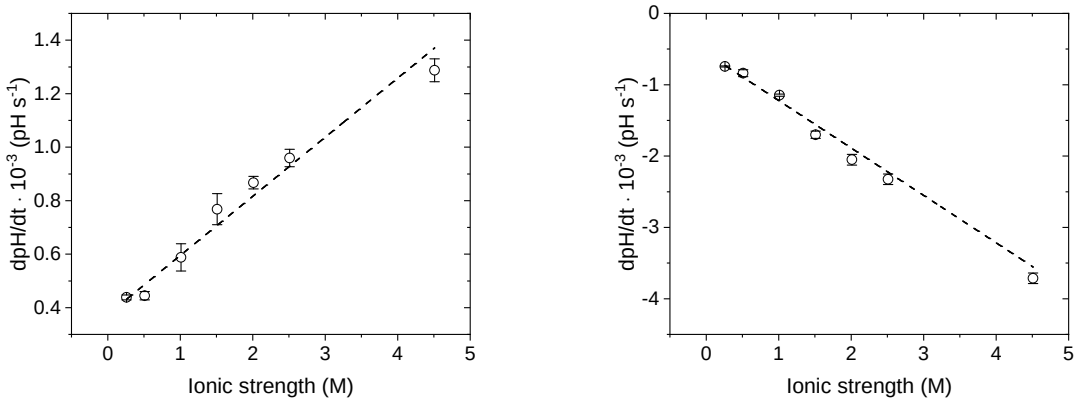

Figure 5.14.: pH change rate of 20 mM MOPS buffer with increasing ionic strength (i.e. Na_2SO_4 concentrations) at working electrode (left) and counter electrode (right) during 10 s of -2 V potential pulse.

5.6. Calibrations

The sensor response depends on the buffer concentration and the initial pH of the sample solution, or rather the distance of the solutions pH from the buffer's pK_a. If one parameter is

kept constant, the other can be calibrated.

5.6.1. MOPS calibrations at pH = pK_a

MOPS buffer measurements (2-100 mM) were recorded at pH 7.2 during 10 s of -2 V pulses. Figure 5.15 shows the resulting calibration curves at working and counter electrode by plotting the maximum rates of pH change against the logarithmic buffer concentration. A single phase exponential function can be fitted for both working and counter electrode compartment.

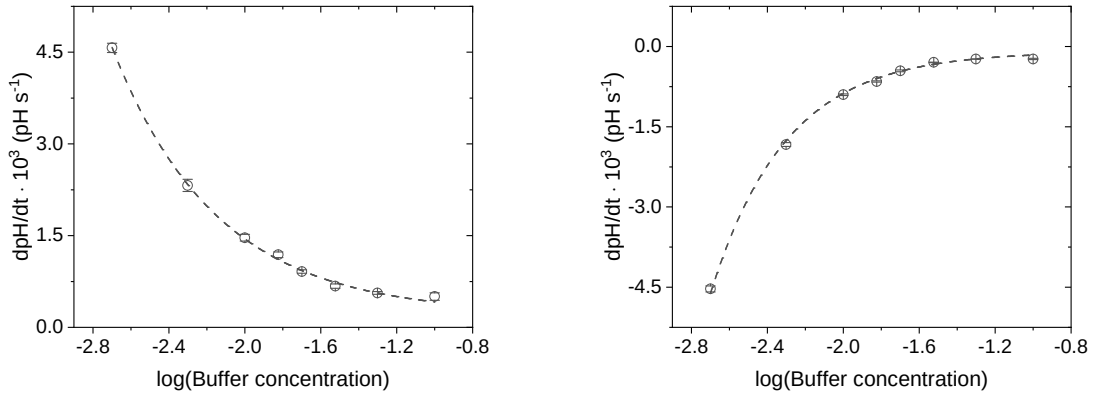

Figure 5.15.: MOPS buffer calibrations at pH 7.2 at working electrode (left) and counter electrode (right). Electrolyte: 0.5 M Na_2SO_4.

5.6.2. pH Dependence of MOPS Calibrations

Figure 5.16 corroborates that the response of the sensor not only depends on buffer concentration but also on the initial pH of the sample solution. Since a buffer works best at its pK_a the smallest changes in pH due to electrochemical water splitting are observed at its pK_a (7.2 at 20 °C). In the working electrode compartment the pH is increased upon applying a negative potential pulse. At higher initial pH values a shift to even higher pH values consequently shifts the buffer's equilibrium even further away from its pK_a.

On the other hand, at pH values below the buffer's pK_a, an increase in pH due to a potential pulse shifts the pH towards the buffer's equilibrium state and therefore constantly increases its buffer capacity during pulsing. Therefore, higher pH change rates are observed at pH = pK_a + 1 than at pH = pK_a- 1.

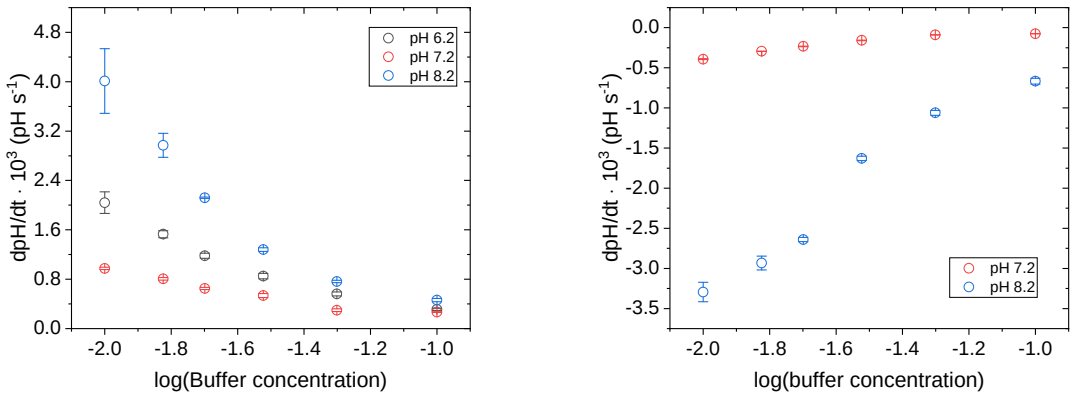

Figure 5.16.: Calibration of 10-100 mM MOPS buffer at pH 6.2, 7.2 and 8.2 at working electrode (left) and counter electrode (right). The pH shift at the counter electrode of the pH 6.2 solution could not be recorded due to limited dynamic range of the optical pH sensor. Electrolyte: 0.5 M Na_2SO_4.

5.6.3. Comparison of Different Measuring Cells

While several measurements in a single cell give reproducible results this is not particularly true throughout different measurement cells. Figure 5.17 shows calibration curves for MOPS buffer at pH 7.2 using three different measuring cells. Since all cells were manufactured by hand, there are slight discrepancies in cell parameters as well as distances between electrodes and sensors. This can lead to different diffusion lengths. As discussed before, different diffusion constants of H^+ and OH^- can lead to small differences in recorded signal relative to the initial pH at the two electrode compartments. However, Figure 5.17 suggests that the factor of different diffusion lengths due to deviations in cell parameters (most importantly distance of optical pH sensor from the electrode) outweighs the factor of diffusion coefficients of acid and base.

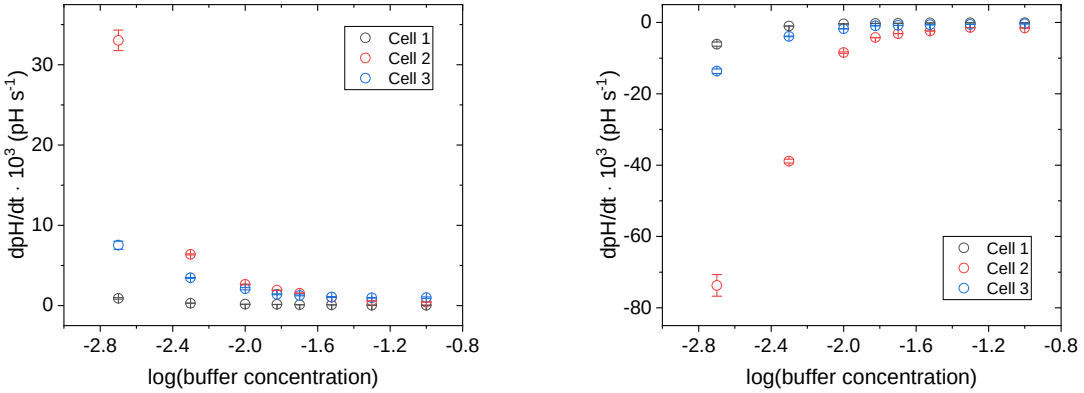

Figure 5.17.: Calibration curves of MOPS buffer (2-100 mM) at pH 7.2 at working electrode (left) and counter electrode (right) in three different measuring cells. Electrolyte: 0.5 M Na_2SO_4.

5.6.4. HEPES Calibration at pH = pK_a

To showcase the response to a different buffer system HEPES buffer measurements (2-100 mM) were recorded at pH 7.55 (= pK_a) during 10 s of -2 V pulses. Figure 5.18 shows the resulting calibration curves at working and counter electrode by plotting the maximum rates of pH change against the logarithmic buffer concentration. A single phase exponential function can be fitted for both working and counter electrode compartment. While the trend looks similar to the one observed in MOPS buffer, especially low buffer concentrations show higher pH change rates, while higher concentrations show quite similar results.

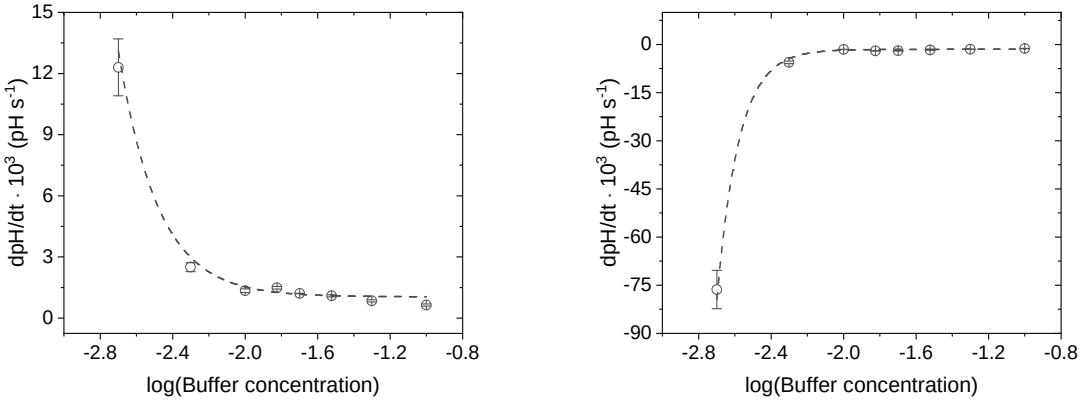

Figure 5.18.: HEPES buffer calibrations at pH 7.55 at working electrode (left) and counter electrode (right). Electrolyte: 0.5 M Na_2SO_4.

Figure 5.19 shows a comparison of MOPS and HEPES calibrations. It has to be stated that a

different measuring cell was used and therefore these results are not comparable with figure 5.18. Here the absolute pH difference of the baseline and peak pH are compared. Again a similar trend can be seen for both buffer substances. Small differences are expected since while the electrolyte and electrolyte concentration in both calibration series is the same, the buffer salts themselves are also dissolved ions in aqueous solution.

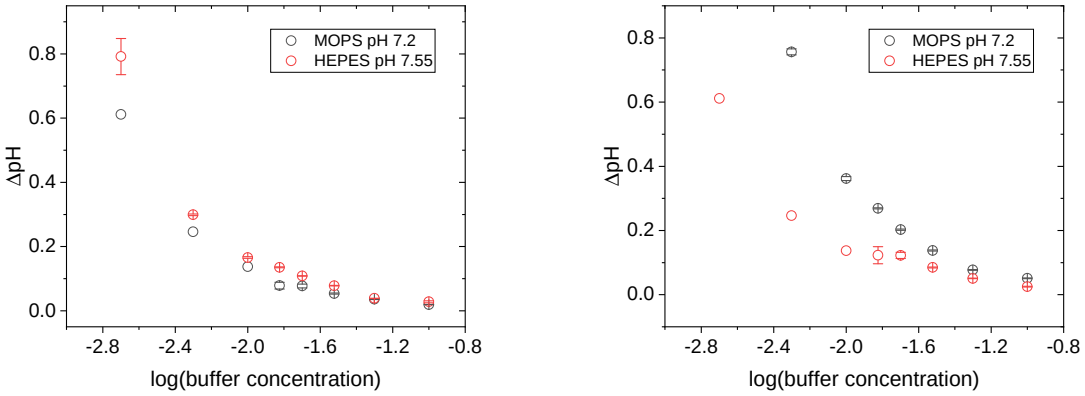

Figure 5.19.: Comparison of ΔpH MOPS and HEPES buffer calibrations at their respective pK_a at working electrode (left) and counter electrode (right). Electrolyte: 0.5 M Na_2SO_4.

Therefore, depending on the conductivity of their respective ions, different buffer salts also contribute different amounts of conductivity to the sample solutions and thus increase the reaction rate at the electrodes to a different extent.

5.6.5. Carbonate Calibration at Environmental pH

Natural samples were taken from the surface and sediment of a quite hard water lake. The ionic composition of those lakes is mostly dominated by calcium and bicarbonate, which enhances the ability of the lake to resist acidification and therefore regulate the environments pH [92]. To mimic the buffer capacity of those natural samples carbonate buffer solutions at concentrations 3.5-15 mM were prepared and the pH adjusted to 8.4.

Figure 5.20 shows the resulting calibration curve of the 10 s of -2 V pulse measurements. It is clearly evident that the measured pH change rates show more deviation from the exponential trend. This is most likely due to a combination of quite low buffer concentration and the initial pH being far from both pK_a values of the carbonate-bicarbonate system. In this pH and concentration range the buffer solutions are very susceptible to added acid and base.

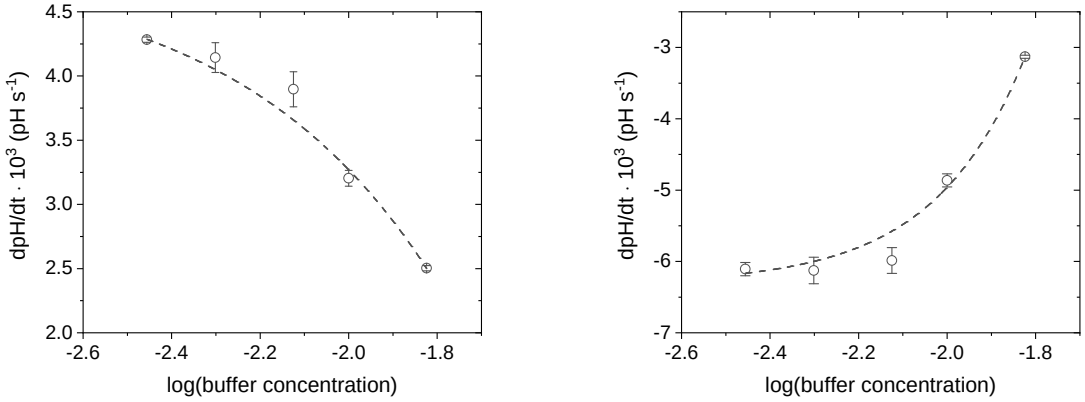

Figure 5.20.: Calibration of 2-15 mM Carbonate-bicarbonate buffer at pH 8.4 at working electrode (left) and counter electrode (right). Electrolyte: 0.5 M Na_2SO_4.

5.7. Surface and Pore Water Samples

Most bodies of water and the underlying sediment show an increase in total alkalinity with increasing sampling depth [93]. Therefore, samples of lake water at different depths were taken. One being surface water and the other one sediment pore water sampled at approx. 0.5 m depth. The samples were centrifuged and filtered to remove any solids and bacteria prior to measurement. Na_2SO_4 was added as electrolyte to achieve a final concentration of 0.5 M. The samples were measured and the pH change during a 10 s of -2 V potential pulse recorded.

5.7.1. Equivalent MOPS at pK_a

The first approach to evaluate the strength of the lake water sample solutions was to compare it with the previously done MOPS calibration (see Figure 5.15). This allows to assess the samples in terms of equivalent MOPS at its pK_a. The calibration curve of the working electrode was used for evaluation. The resulting concentration are listed in Table 5.1. The obtained value of the surface water sample is out of calibration range. However, it can be clearly seen that there is increased buffer capacity in the pore water sample, which is in accordance with expectations.

In order to obtain comparable values like total alkalinity (TA) in terms of meq/L TA or mg/L $CaCO_3$ the calibration samples including the electrolyte were titrated with 0.5 N HCl to an endpoint of pH 4.5. The amount of acid needed to reach this endpoint was recorded by a digital buret and can be converted to total alkalinity in terms of meq/L by using equation 5.8. It is important that the concentration of the used acid is expressed in normality instead of molarity, since some acids can donate more than one proton. In this case however, the molarity and

Table 5.1.: Buffer capacity detection in water samples in terms of mmol MOPS per litre at its pK_a.

Sample	Buffer Capacity (mM MOPS at pK_a)
Surface water	1.88 ± 0.03 [a]
Pore water	2.42 ± 0.05

[a] out of calibration range

normality is the same since HCl was used and only one proton per molecule can be participate in the neutralization reaction.

$$TA\ (meq/L)\ =\ \frac{V(acid)\cdot c(acid)}{V(sample)} \tag{5.8}$$

Figure 5.21 shows the linear correlation of total alkalinity with increasing MOPS concentration. The slope is close to 0.5 which is to be expected because the sample solutions were titrated starting from the buffers pK_a, i.e. pH 7.2. According to the Henderson-Hasselbalch equation at $pH = pK_a$ half of the buffer molecules are already protonated. Therefore, an x-fold increase of buffer concentration should show an 0.5x-fold increase in total alkalinity.

Usually total alkalinity values are reported in mg/L $CaCO_3$. Considering every molecule of $CaCO_3$ has the ability to neutralize two protons it represents two miliequivalents of alkalinity. In combination with the molecular weight of $CaCO_3$ the alkalinity equivalents can be converted to mg/L by using equiation 5.9.

$$TA(mg/L\ CaCO_3)\ =\ TA(meq/L)\cdot\frac{1\ mmol\ CaCO_3}{2\ meq\ Alkalinity}\cdot\frac{100\ mg\ CaCO_3}{1\ mmol\ CaCO_3} \tag{5.9}$$

The results are shown in Table 5.2. Although there is a noticeable difference between pore and surface water, there are substantial differences to the values measured by conventional titration. In general this method is more prone to error because it is dependent on two independent measurements. Furthermore, the titration measurement was performed at higher temperature (24 °C) compared to the combined optical-electrochemical measurements (21 °C). Since the pK_a of the buffer is dependent on temperature small differences in temperature might significantly change the pK_a and therefore alter the results [94].

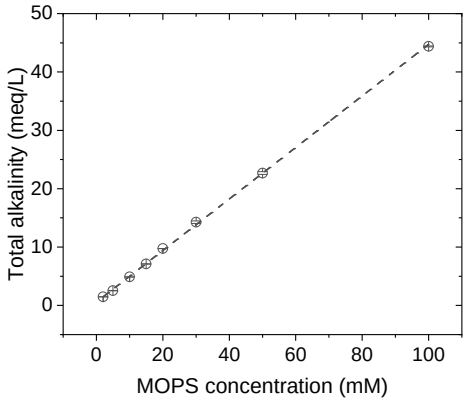

Figure 5.21.: Determination of total alkalinity of MOPS buffer (2, 5, 10, 15, 20, 30, 50 and 100 mM) by titration with 0.1 N hydrochloric acid).

Table 5.2.: Alkalinity detection in water samples obtained by titration of MOPS calibration values. Values in brackets indicate alkalinity expressed as mg/L carbonate.

Sample	Alkalinity (meq/L)	
	Our method	Titration
Surface water	1.41 ± 0.01 (70.6)	6.18 ± 0.01
Pore water	1.64 ± 0.02 (82.5)	9.90 ± 0.01

5.7.2. Carbonate Buffer Calibration

Since the carbonate buffer system is the most abundant in most natural water bodies the obtained pH change rates of the taken samples were compared with the recorded carbonate buffer calibration at environmental pH. The results are given in Table 5.3. It is important to note that in this table alkalinity is displayed in mmol HCO_3^- per litre sample. Since every molecule of HCO_3^- is able to neutralize one proton, the terms mM HCO_3^- and meq/L both terms can be used interchangeably.

Compared to the previously presented method this approach shows generally better results. However, there still is a is a small offset to the titration results. This is most likely due to the fact that titration and measurement in the proposed setup were not performed at the same time. Storage and handling can lead to loss of integrity in the sample due to re-equilibration with atmospheric CO_2, which can lead to deviations in the results ($< 20\,\%$) [26]. Also, the natural samples were compared to pure bicarbonate stocks. Since many other buffering species may be present in these samples (e.g. boric acid, ammonia, silicates, etc.) it is not unexpected that higher buffer capacities (i.e. bicarbonate concentrations) were measured. Further deviations

may result from using ultra pure water for the calibration stocks. In the natural samples, however, various other ions are dissolved which can contribute to the general conductivity of the sample. Variations of conductivity can change the reaction rate at the electrode and therefore alter the measured pH change. Furthermore, freshwater contains several dissolved organic and inorganic substances. If any of those are redox active and can be oxidized or reduced in the applied potential range some of the electrons intended for the electrolysis of water are used for other redox processes and therefore decrease the water-splitting reaction rate.

Table 5.3.: Alkalinity detection in water samples obtained using carbonate buffer calibration. Values in brackets indicate alkalinity expressed as mg/L carbonate.

Sample	Alkalinity (mM HCO_3^-)	
	Our method	Titration
Surface water	10.1 ± 0.3 (505)	6.18 ± 0.01
Pore water	13.5 ± 0.2 (674)	9.90 ± 0.01

5.8. pK_a Determination of MOPS at Ambient Conditions

As discussed before, the sensor response depends on buffer concentration and distance of the solutions initial pH from the buffer's pK_a. Thus, at constant buffer concentration the buffer's pK_a can be determined. Therefore, 10 s of a -2 V pulse were applied to a solution of 20 mM MOPS and 0.5 M Na_2SO_4 at various initial pH values (6.9, 7.2, 7.5, 7.8 and 8.2) at ambient conditions (21 °C). Figure 5.22 shows the recorded maximum pH change rates at different pH values at both electrodes. Since generally a buffer works best at its pK_a, the lowest rate of pH change corresponds to the apparent pK_a at of the buffer solution at the current conditions. The lowest rate and therefore the apparent pK_a was observed at pH 7.2-7.3.

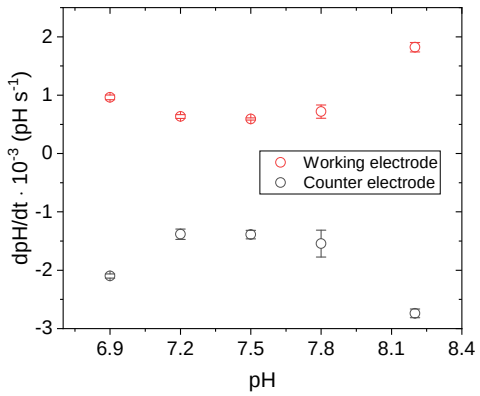

Figure 5.22.: Determination of apparent pK_a of MOPS buffer.

To verify the determined value a conventional titration of 20 mM MOPS and 0.5 M Na_2SO_4 adjusted to pH 11 with 0.1 N HCl was performed. The resulting pK_a was 7.21. However, pK_a values are prone to fluctuate due to changes in temperature and ionic strength. In general MOPS buffer shows quite small variations of pK_a due to temperature change but still a change of -0.013 dpK_a/dT is observed [95]. For comparison the obtained value by titration was corrected to 7.25 for 21 °C. This corresponds well with the value of 7.2-7.3 measured in the proposed system. Figure 5.23 shows the data obtained from the volumetric titration and both the original and temperature corrected pK_a measured by titration displayed in the combined optical and electrochemical pK_a determination plot.

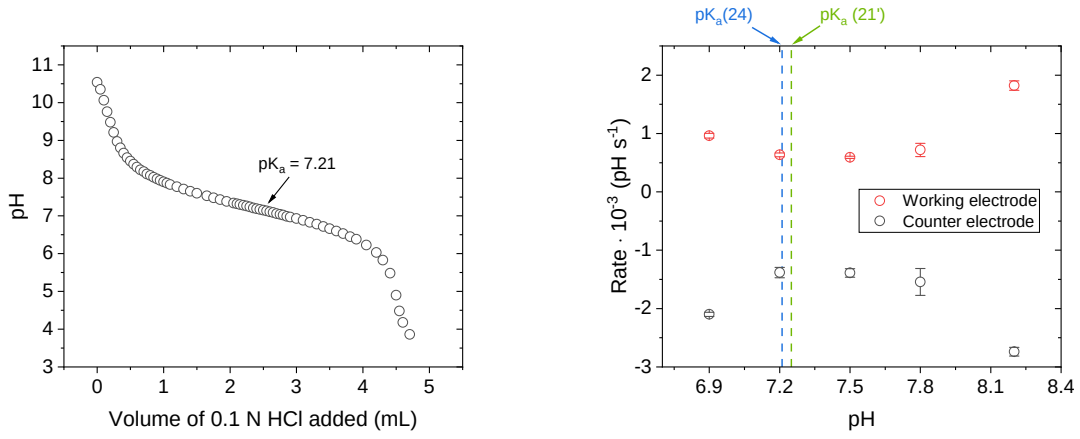

Figure 5.23.: Determination of MOPS pK_a by volumetric titration with 0.1 N HCl at 24 °C (left) and determination of MOPS pK_a using the proposed system (right). The dashed blue line, denoted pK_a (24), shows the pK_a determined by titration at 24 °C, while the green line, denoted pK_a (21') shows the temperature corrected (21 °C) pK_a value.

6. Characterization of Quinones

Alternatively to water electrolysis a localized pH change can be achieved using redox induced pH shifting by electro acids/bases. A prominent example for molecules that can reversible capture and release protons upon electrochemical stimulus are quinones. In the following section two potential quinone-based molecules are investigated regarding electrochemical reversibility and stability in aqueous solution.

6.1. Electrochemical Characterization of Quinones

Two quinones, 1,4-benzoquinone (BQ) and anthraquinone-2,7-disulfonic acid (AQDS), have been investigated (Figure 6.1). Therefore, cyclic voltammograms in aqueous media were recorded using different electrode systems (screen printed gold and screen printed carbon) and supporting electrolytes (KCl and KNO_3).

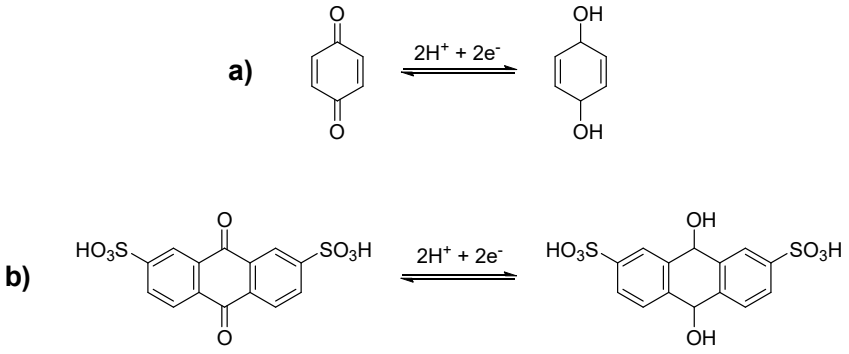

Figure 6.1.: Redox process accompanied by protonation/deprotonation of studied quinones. a) 1,4-benzoquinone b) anthraquinone-2,7-disulfonic acid.

The CVs were analysed in terms of peak potentials and peak currents. To determine corrected peak current values, background current baselines were extrapolated and subtracted from the measured peak current values, as exemplified in Figure 6.2 (left). Diffusion control and Nernstian reversibility of the electron transfer reaction was evaluated by recording several cyclic voltammograms at different scan rates (10, 50, 100 and 500 mV/s). The peak current I_p for reversible reactions of free diffusing species is given by equation 6.1 [96]. A linear

correlation of peak currents with $v^{1/2}$ indicates a fast electron transfer in diffusion controlled redox reactions.

$$i_p = 0.4463 \cdot \left(\frac{F^3}{RT}\right)^{\frac{1}{2}} \cdot n^{\frac{3}{2}} \cdot A \cdot D_0^{\frac{1}{2}} \cdot C_0^* \cdot v^{\frac{1}{2}} \tag{6.1}$$

F represents the Faraday constant, R the gas constant, T the temperature, n the number of electrons transferred, A the area of the electrode, D_0 the diffusion coefficient, C_0^* the bulk concentration of the analyte and v the scan rate. For reversible reactions a peak current ratio close to unity is expected. The formal redox potential E_f^0 is the midpoint potential between the two peak potentials in each CV, in this case measured against a Ag/Ag^+ pseudoreference electrode. Both, current ratio and formal redox potential for a scan rate of 10 mV/s are shown in Table 6.1 and Table 6.2 for gold and carbon electrodes, respectively.

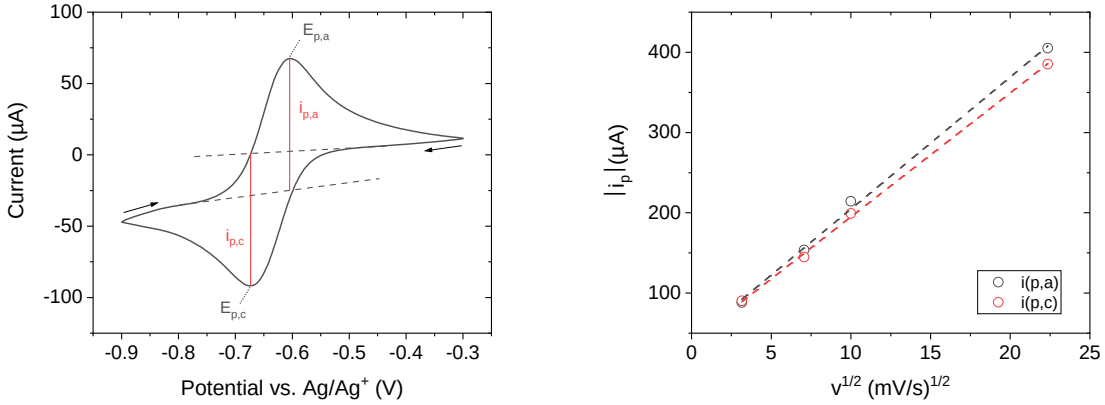

Figure 6.2.: Data evaluation of individual CVs (left) and resulting peak current versus square root of scan rate plot to showcase diffusion control (right). Here the evaluation of 1 mM AQDS in 0.1 M KCl on screen printed gold electrodes is shown.

Table 6.1.: Comparison of formal redox potential, peak separation and current ratio for BQ and AQDS on screen printed gold electrodes measured at 10 mV/s.

Sample	Electrolyte	Peak sep. (mV)	E_f^0 (mV)	Current ratio
1 mM BQ	- [a]	692	68	0.98
1 mM AQDS	0.1 M KNO_3	74	-671	0.97
10 mM AQDS	0.1 M KCl	72	-64	0.97
100 mM AQDS	0.1 M KNO_3	82	-628	0.88

[a] instead of an conventional electrolyte 0.1 M phosphate buffer (pH 7) was used

All measured samples showed linear correlation between peak currents and the square root of the scan rate, indicating diffusion controlled reactions (individual plots can be seen in the appendix). However, all samples show increasing peak separation with increasing scan rate, indicating that the rate of electron transfer becomes comparable to the rate of mass transport. Therefore, both quinones undergo a quasi-reversible electron transfer.

AQDS shows peak current ratios close to one and peak potential separations close to 59 mV on gold electrodes, which would be the expected value for a reversible one-electron-transfer [96]. However, slightly higher values also indicate a system which is not completely reversible but rather quasi-reversible. Changing the electrolyte solution from KCl to KNO_3 did not result in a significant change in terms of peak separation or peak currents.

BQ on the other hand shows a very drastic separation of oxidation and reduction peak. Figure 6.3 shows a comparison of two cyclic voltammograms of BQ and AQDS on screen printed gold electrodes. While both show similar peak current ratios, the peak separation is much more pronounced in the cyclic voltammogramm of BQ. It has to be stated, that while for AQDS a regular electrolyte (KNO_3) was used, for BQ no electrolyte per se, like KCl or KNO_3 was used. Instead a 0.1 M phosphate buffer, in the form of sodium salts was used. Therefore, while different salts were used a similar amount of supporting electrolyte was in both samples.

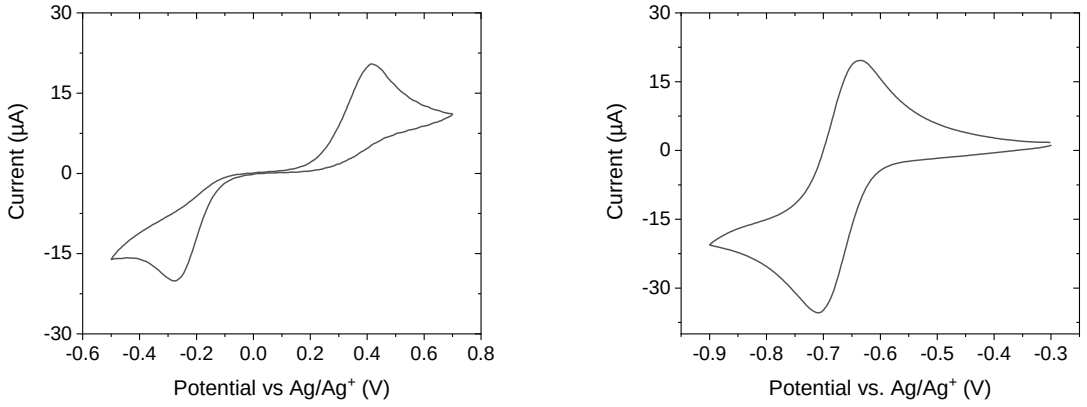

Figure 6.3.: Comparison of cyclic voltammogramms of BQ (left) and AQDS (right) on screen printed gold electrodes (10 mV/s).

While the CV of AQDS on gold electrodes looks reversible when only looking at the first cycles, after about 10 cycles a brown-black deposit forms mainly on the working electrode. To exclude instabilities of the electrodes and electrolyte, several cycles of cyclic voltammetry were performed in pure 0.1 M KNO_3 solution and no deposit could be observed. Therefore, the deposit must result from the some kind of interaction between the oxidized or reduced form of AQDS with the electrodes.

Table 6.2.: Comparison of formal redox potential, peak separation and current ratio for BQ and AQDS on screen printed carbon electrodes measured at 10 mV/s.

Sample	Electrolyte	Peak sep. (mV)	E_f^0 (mV)	Current ratio
100 mM AQDS	0.1 M KNO_3	236	-423	0.77
100 mM BQ	0.1 M KNO_3	194	-628	0.74

Thus, carbon was used as an alternative electrode material. After several cycles of cyclic voltammetry no deposit could be observed. Figure 6.4 illustrates cyclic voltammograms of BQ and AQDS on screen printed carbon electrodes. Again a linear correlation between peak currents and the square root of the scan rate could be found. Also a smaller peak separation and thus a faster electron transfer compared to the experiments on gold electrodes was observed for BQ. AQDS on the other hand showed increased peak separation. Both quinones presented decreased peak current ratios on carbon electrodes, indicating a decrease in Nernstian reversibility.

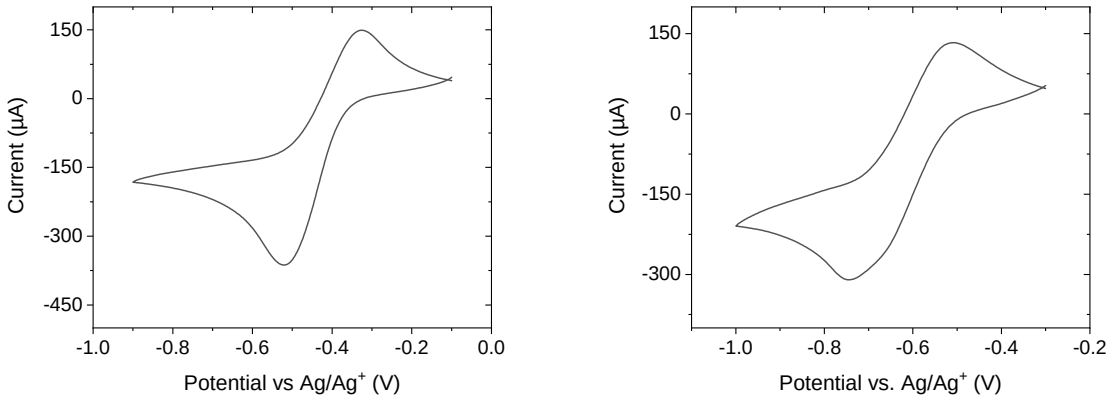

Figure 6.4.: Comparison of cyclic voltammogramms of BQ (left) and AQDS (right) on screen printed carbon electrodes (10 mV/s).

6.1.1. Influence of Buffer Concentration and pH

The redox chemistry of quinones is best described as a 2 e^-, 2 H^+ reaction resulting in a hydroquinone product. A change in redox state will thus be accompanied by a local change in pH in unbuffered solutions [97]. Since protons are associated with the overall redox process, also the redox potential is pH dependent. This leads to a continuously changing redox potential throughout the reduction or oxidation process in unbuffered solutions [98].

Figure 6.5 shows cyclic voltammograms of BQ in different concentrations of phosphate buffer (0.1, 1 and 2.5 M) and at different pH values (0.1 M phosphate buffer: pH 5, 6 and 7). By

increasing the buffer concentration from 0.1 M to 2.5 M the voltammogram and therefore the formal potential shifts by 69 mV to higher potentials. This indicates that the reaction is thermodynamically easier facilitated in the presence of a buffer. On the other hand, a decrease in peak current ratio implies that the electron transfer is kinetically much slower. In addition, with increasing amount of buffering species lower peak currents are observed in both scan directions.

Changing the pH of the used buffer solution did not show drastic differences in formal potential or peak current ratio. However, at lower pH a bigger peak separation was observed, indicating that at higher or near neutral pH the system is kinetically favoured.

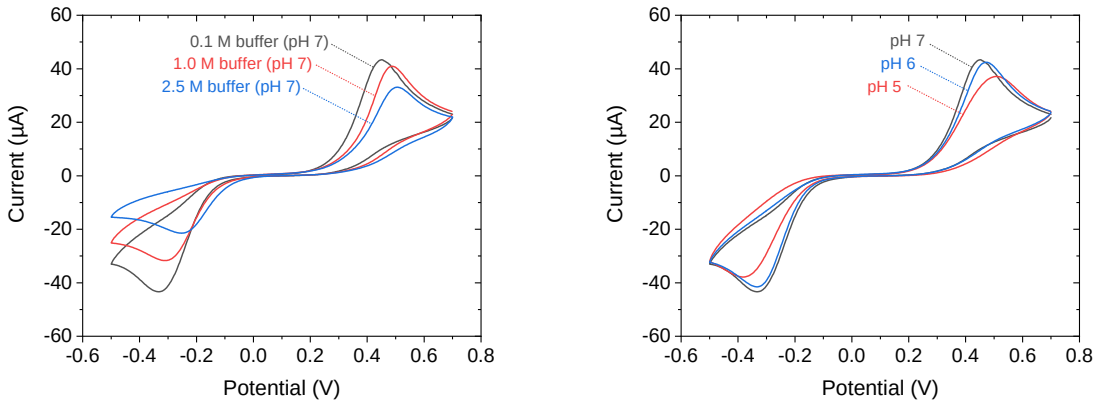

Figure 6.5.: Evaluation of the influence of buffer concentration (left) and initial pH (right) on the cyclic voltammetry behaviour of 1 mM BQ on gold electrodes

6.1.2. Electrochemical Stability Cycling

When used as a pH shifting platform the stability of the used electroactive species is crucial for reproducibility and a reliable setup. To access the electrochemical stability of the quinones 10 cycles of cyclic voltammetry on screen printed carbon electrodes were recorded (Figure 6.6). Both show a significant decrease in current response both in anodic and cathodic direction.

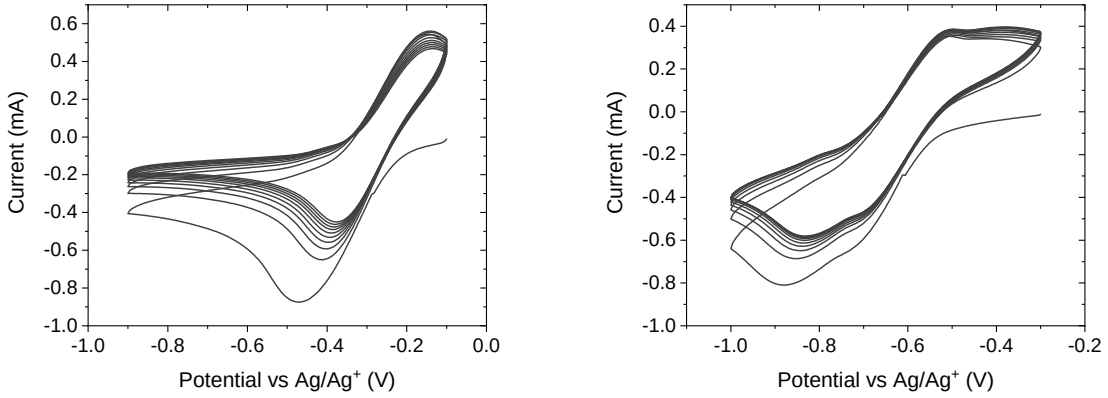

Figure 6.6.: 10 cycles of cyclic voltammetry of BQ (left) and AQDS (right) on screen printed carbon electrodes in 0.1 M KNO_3.

To some extent this is in accordance with expectations since the system is not stirred during the measurement and therefore the transport of molecules from the bulk to the electrodes is dependent on diffusion.

Figure 6.7 illustrates peak currents in anodic and cathodic direction throughout 10 consecutive cycles. Comparison of the peak currents indicates that BQ initially shows higher peak currents in the both sweep directions. Most importantly however, AQDS shows significantly smaller changes in peak currents in both scan directions after the initial few cycles.

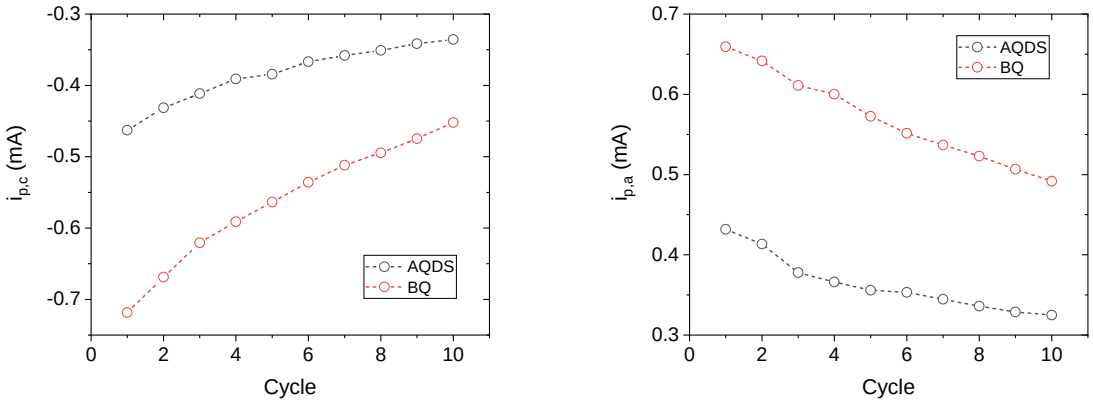

Figure 6.7.: Cathodic (left) and anodic (right) peak currents over 10 cycles of cyclic voltammetry.

This indicates that AQDS is overall the more electrochemically stable molecule in aqueous solution. Furthermore, unsubstituted benzoquinones are known to be quite chemically unstable in aqueous solutions. Figure 6.8 shows how BQ and similar quinones with vulnerable attack

sites can undergo gem-diol formation (reversible, but inhibits kinetics) and Michael addition (irreversible) and subsequent tautomerization. While the resulting molecules might still be electrochemically active, Michael addition to quinones generally substantially decreases the performance of the quinone and also might make the molecules susceptible to further reactions with water and therefore decrease performance even more. This renders substituted quinones like AQDS in general better candidates in case of stability [99].

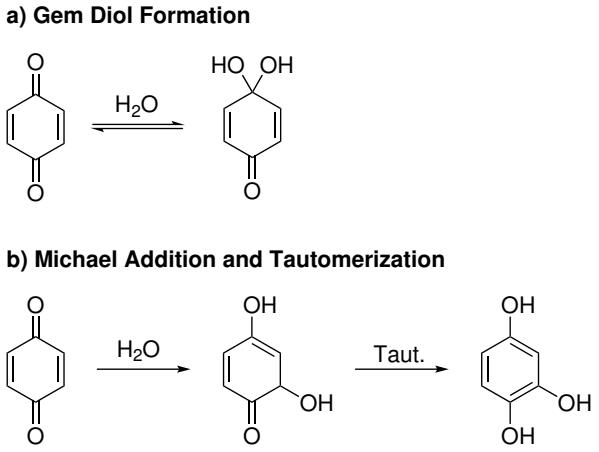

Figure 6.8.: Possible decomposition reactions of BQ in aqueous media.

6.2. pK_a determination of AQDS

Several absorption spectra of AQDS in buffered solution (pH 6-10) were recorded. Figure 6.9 shows the normalized absorption spectrum and the calibration curve of the absorbance at 479 nm versus pH. The apparent pK_a value measured at 21 °C of 7.56 is in accordance with literature. However, since quinones bare two protic groups, two pK_a values would be expected. While the electrochemical approach leads to two different pK_a values (7.6 and 10.6 [100]), apparently only one of those protonation steps is accompanied by a change in optical properties. Therefore, using this method allows the determination of only one pK_a value.

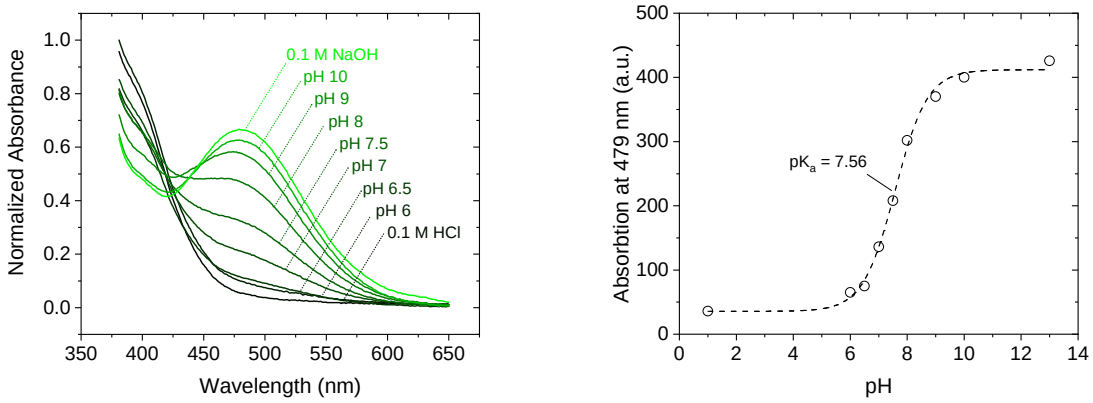

Figure 6.9.: Normalized absorption of 1 mM AQDS in water (left) and absorption at 479 nm as a function of pH (right).

7. Conclusion and Outlook

In this thesis a novel dynamic sensor for buffer capacity combining electrochemical methods with optical sensors has been developed. Various cell parameters (e.g. applied potential, pulse time, supporting electrolyte, etc.) and different setups have been investigated in order to build a system which delivers reproducible results. Furthermore, instead of relying on passive measurement of pH a dynamic approach was used by measuring the rate of pH change instead of using absolute pH values. This allowed to bypass the requirement of the sensor to fully equilibrate before read-out and therefore drastically decrease the required time per measurement. Calibrations with different buffer concentrations in various buffer systems (MOPS, HEPES and carbonate) have been performed, showing a similar results throughout the measurements. Furthermore, the system allowed to detect the apparent pK_a of the investigated buffer at the present conditions (i.e. temperature, ionic strength).

Practical application of the sensing principle has been tested by using it to measure lake pore water and surface water samples. As expected a clear difference in buffer capacity was observable between the two samples, with the pore water sample having significantly higher buffer capacity. The results have been validated by conventional alkalinity titrations (approx. 30 % relative deviation).

Furthermore, two electro acids/bases, 1,4-benzoquinone (BQ) and anthraquinone-2,7-disulfonic acid (AQDS), have been investigated as possible candidates for redox induced pH switching. Generally, AQDS proofed to be the chemically more stable compound with superior electrochemical reversibility, which makes it a promising candidate for reversible localized redox induced pH control.

For further research, these electro acids/bases can be employed as proton pump in the existing buffer capacity measuring system. This would enable pH shifting without potential bubble generation as a limiting factor. However, more research must be conducted towards how these molecules can be implemented in the system (e.g. incorporation of a polymer film with a high quinone load on top of the electrode or direct coupling of the quinone onto the carbon electrodes).

Moreover, establishing controllable and reproducibly pH gradients would allow further combination of optical sensors with electrochemical methods. This would allow development of activatable sensors than are capable of measuring an additional parameter after electrochemical activation, e.g. ammonia sensors that can not only measure free ammonia but also total ammonia nitrogen (TAN). Nowadays optical ammonia sensors only measure either free ammonia or its conjugated acid ammonium. These two are in equilibrium and the relative amount of the respective species is dependent on pH. Combination of an optical ammonia sensor with an electrochemical pH shifting platform would allow the sensor to be activatable to measure a second parameter. In other words the sensor would measure free ammonia while no potential is applied and as soon as the pH is shifted due to electrochemical stimulus the equilibrium between ammonia and ammonium is shifted due to electrochemically induced pH shift. If the pH is increased, ammonium is converted to ammonia and the increased total level of ammonia would correspond to TAN. Similarly, free CO_2 could be measured in absence of applied potential and after electrochemical acidification total inorganic carbon could be assessed.

References

[1] Laurent Bouffier and Thomas Doneux. “Coupling electrochemistry with in situ fluorescence (confocal) microscopy”. In: *Current Opinion in Electrochemistry* 6.1 (2017), pp. 31–37.

[2] P. Audebert and F. Miomandre. “Electrofluorochromism: From molecular systems to set-up and display”. In: *Chemical Science* 4.2 (2013), pp. 575–584.

[3] Jingwei Sun, Yani Chen, and Ziqi Liang. “Electroluminochromic Materials and Devices”. In: *Advanced Functional Materials* 26.17 (2016), pp. 2783–2799.

[4] Amerigo Beneduci et al. “Highly fluorescent thienoviologen-based polymer gels for single layer electrofluorochromic devices”. In: *Advanced Functional Materials* 25.8 (2015), pp. 1240–1247.

[5] F Miomandre et al. “Electrofluorochromism of a ruthenium complex investigated by time resolved TIRF microscopy coupled to an electrochemical cell”. In: *Electrochemistry Communications* 20.1 (2012), pp. 83–87.

[6] Daniel Martín-Yerga et al. “Time-Resolved Luminescence Spectroelectrochemistry at Screen-Printed Electrodes: Following the Redox-Dependent Fluorescence of [Ru(bpy) 3] 2+”. In: *Analytical Chemistry* 89.20 (2017), pp. 10649–10654.

[7] Wei Xu, Kaiyu Fu, and Paul W. Bohn. “Electrochromic sensor for multiplex detection of metabolites enabled by closed bipolar electrode coupling”. In: *ACS Sensors* 2.7 (2017), pp. 1020–1026.

[8] Sutida Jansod et al. “Colorimetric Readout for Potentiometric Sensors with Closed Bipolar Electrodes”. In: *Analytical Chemistry* 90.11 (2018), pp. 6376–6379.

[9] Kwok-Fan Chow et al. “A Large-Scale, Wireless Electrochemical Bipolar Electrode Microarray”. In: *Journal of the American Chemical Society* 131.24 (2009), pp. 8364–8365.

[10] Laurent Bouffier et al. “Imaging Redox Activity at Bipolar Electrodes by Indirect Fluorescence Modulation”. In: *Analytical Chemistry* 86.8 (2014), pp. 3708–3711.

[11] Guoqiang Ding et al. “Electrofluorochromic detection of cyanide anions using a benzothiadiazole-containing conjugated copolymer”. In: *Chem. Commun.* 50.6 (2014), pp. 655–657.

[12] Gary D. Christian, Purnendu K. Dasgupta, and Kevin A. Schug. *Analytical chemistry, fourth edition (Christian, Gary D.)* Vol. 7. Wiley-VCH Verlag GmbH & Co. KGaA, 2013.

[13] Edward T. Urbansky and Michael R. Schock. "Understanding, Deriving, and Computing Buffer Capacity". In: *Journal of Chemical Education* 77.12 (2000), p. 1640.

[14] Jorge G. Ibanez et al. *Environmental Chemistry*. New York, NY: Springer New York, 2007.

[15] A. G. Dickson. "An exact definition of total alkalinity and a procedure for the estimation of alkalinity and total inorganic carbon from titration data". In: *Deep Sea Research Part A, Oceanographic Research Papers* 28.6 (1981), pp. 609–623.

[16] *Acid-Base Disorders*. 2014.

[17] Joseph R Casey, Sergio Grinstein, and John Orlowski. "Sensors and regulators of intracellular pH". In: *Nature Reviews Molecular Cell Biology* 11.1 (2010), pp. 50–61.

[18] Ray R. Weil and Nyle C. Brady. *The Nature and Properties of Soil*. 15th ed. Pearson Education, 2017.

[19] Rebecca E. Haling et al. "Effect of soil acidity, soil strength and macropores on root growth and morphology of perennial grass species differing in acid-soil resistance". In: *Plant, Cell & Environment* 34.3 (2011), pp. 444–456.

[20] Celia Y Chen and Edward G Durbin. "Effects of pH on the growth and carbon uptake of marine phytoplankton". In: *Marine Ecology Progress Series* 109 (1994), pp. 83–94.

[21] Kristy J. Kroeker et al. "Impacts of ocean acidification on marine organisms: quantifying sensitivities and interaction with warming". In: *Global Change Biology* 19.6 (2013), pp. 1884–1896.

[22] Jianguo Wang et al. "An Electrochemical Approach for the Direct Measurement of Buffer Capacity". In: *Journal of The Electrochemical Society* 161.9 (2014), H555–H557.

[23] Nadezda Pankratova et al. "Local Acidification of Membrane Surfaces for Potentiometric Sensing of Anions in Environmental Samples". In: *ACS Sensors* 1.1 (2016), pp. 48–54.

[24] Majid Ghahraman Afshar et al. "Direct Alkalinity Detection with Ion-Selective Chronopotentiometry". In: *Analytical Chemistry* 86.13 (2014), pp. 6461–6470.

[25] William W. Bennett et al. "A colorimetric DET technique for the high-resolution measurement of two-dimensional alkalinity distributions in sediment porewaters". In: *Chemosphere* 119 (2015), pp. 547–552.

[26] Maria Cuartero et al. "In Situ Detection of Species Relevant to the Carbon Cycle in Seawater with Submersible Potentiometric Probes". In: *Environmental Science & Technology Letters* 4.10 (2017), pp. 410–415.

[27] Alexander Wiorek et al. “Polyaniline Films as Electrochemical-Proton Pump for Acidification of Thin Layer Samples”. In: *Analytical Chemistry* (2019), acs.analchem.9b03402.

[28] G Mistlberger et al. “Photodynamic optical sensor for buffer capacity and pH based on hydrogel-incorporated spiropyran”. In: *Chemical Communications* 51.20 (2015), pp. 4172–4175.

[29] Renjie Wang et al. “Distance and Color Change Based Hydrogel Sensor for Visual Quantitative Determination of Buffer Concentrations”. In: *ACS Sensors* 4.4 (2019), pp. 1017–1022.

[30] Mingyong Wang et al. “The intensification technologies to water electrolysis for hydrogen production – A review”. In: *Renewable and Sustainable Energy Reviews* 29 (2014), pp. 573–588.

[31] Shichao Du et al. “Co3O4 nanocrystal ink printed on carbon fiber paper as a large-area electrode for electrochemical water splitting”. In: *Chemical Communications* 51.38 (2015), pp. 8066–8069.

[32] Haiyan Jin et al. “In situ Cobalt–Cobalt Oxide/N-Doped Carbon Hybrids As Superior Bifunctional Electrocatalysts for Hydrogen and Oxygen Evolution”. In: *Journal of the American Chemical Society* 137.7 (2015), pp. 2688–2694.

[33] Yongye Liang et al. “Co3O4 nanocrystals on graphene as a synergistic catalyst for oxygen reduction reaction”. In: *Nature Materials* 10.10 (2011), pp. 780–786.

[34] Yinlong Zhu et al. “SrNb 0.1 Co 0.7 Fe0.2O3- δ Perovskite as a Next-Generation Electrocatalyst for Oxygen Evolution in Alkaline Solution”. In: *Angewandte Chemie International Edition* 54.13 (2015), pp. 3897–3901.

[35] Long Chen et al. “Base–acid hybrid water electrolysis”. In: *Chemical Communications* 52.15 (2016), pp. 3147–3150.

[36] Hongbo Zhou, Gang Li, and Shuhuai Yao. “A droplet-based pH regulator in microfluidics”. In: *Lab Chip* 14.11 (2014), pp. 1917–1922.

[37] Catherine R Cabrera, Bruce Finlayson, and Paul Yager. “Formation of Natural pH Gradients in a Microfluidic Device under Flow Conditions: Model and Experimental Validation”. In: *Analytical Chemistry* 73.3 (2001), pp. 658–666.

[38] Jun Suzurikawa et al. “Microscale pH gradient generation by electrolysis on a light-addressable planar electrode”. In: *Sensors and Actuators B: Chemical* 149.1 (2010), pp. 205–211.

[39] Kateřina Macounová et al. “Generation of Natural pH Gradients in Microfluidic Channels for Use in Isoelectric Focusing”. In: *Analytical Chemistry* 72.16 (2000), pp. 3745–3751.

[40] Sven O Krabbenborg et al. “Reactivity mapping with electrochemical gradients for monitoring reactivity at surfaces in space and time”. In: *Nature Communications* 4.1 (2013), p. 1667.

[41] Christopher Batchelor-McAuley et al. “Voltammetric Characterization of DNA Intercalators across the Full pH Range: Anthraquinone-2,6-disulfonate and Anthraquinone-2-sulfonate”. In: *The Journal of Physical Chemistry B* 114.11 (2010), pp. 4094–4100.

[42] Alexey S. Stepanov et al. “Redox induced pH-switch of Tb(III) centered luminescence of Tb(III) complex with p-sulfonatothiacalix[4]arene”. In: *Electrochemistry Communications* 12.5 (2010), pp. 703–705.

[43] Gabriel Antonio S. Minero et al. “Electronic pH switching of DNA triplex reactions”. In: *RSC Advances* 5.35 (2015), pp. 27313–27325.

[44] Kristina Wedege et al. “Organic Redox Species in Aqueous Flow Batteries: Redox Potentials, Chemical Stability and Solubility”. In: *Scientific Reports* 6.1 (2016), p. 39101.

[45] N Fomina et al. “An electrochemical platform for localized pH control on demand”. In: *Lab on a Chip* 16.12 (2016), pp. 2236–2244.

[46] Zhao Ping et al. “Protonation and electrochemical redox doping processes of polyaniline in aqueous solutions: Investigations using in situ FTIR-ATR spectroscopy and a new doping system”. In: *Journal of the Chemical Society, Faraday Transactions* 93.1 (1997), pp. 121–129.

[47] Allen J. Bard and Faulkner Larry R. *Electrochemical Methods - Fundamentals and Applications*. Vol. 2. 2001.

[48] Cynthia G. Zoski. *Handbook of electrochemistry*. 2007.

[49] Richard G Compton and Craig E Banks. *Understanding Voltammetry*. IMPERIAL COLLEGE PRESS, 2010, pp. 107–151.

[50] Noémie Elgrishi et al. “A Practical Beginner’s Guide to Cyclic Voltammetry”. In: *Journal of Chemical Education* 95.2 (2018), pp. 197–206.

[51] Bernard Valeur and Mário Nuno Berberan-Santos. *Molecular Fluorescence*. Vol. 1. Weinheim, Germany: Wiley-VCH Verlag GmbH & Co. KGaA, 2001.

[52] Joseph R. Lakowicz. *Principles of fluorescence spectroscopy*. Vol. 3. Boston, MA: Springer US, 2006, pp. 1–954.

[53] Michael Kasha. “Characterization of Electronic Transitions in Complex Molecules”. In: *Discussion of the Faraday Society* 9.14 (1950).

[54] George Gabriel Stokes. “On the Change of Refrangibility of Light”. In: *Philosophical Transactions of the Royal Society of London* 142 (1852), pp. 463–562.

[55] Glenn A. Crosby and James N. Demas. “Measurement of photoluminescence quantum yields. Review”. In: *The Journal of Physical Chemistry* 75.8 (1971), pp. 991–1024.

[56] Otto S. Wolfbeis and Bernhard M. Weidgans. *Fiber Optic Chemical Sensors and Biosensors: a View Back*. November 1991. 2006, pp. 17–44.

[57] Florinel-Gabriel Bănică. *Chemical Sensors and Biosensors*. Chichester, UK: John Wiley & Sons, Ltd, 2012.

[58] Colette McDonagh, Conor S Burke, and Brian D. MacCraith. “Optical Chemical Sensors”. In: *Chemical Reviews* 108.2 (2008), pp. 400–422.

[59] Sergey M Borisov and Otto S Wolfbeis. “Optical Biosensors”. In: *Chemical Reviews* 108.2 (2008), pp. 423–461.

[60] Peter Gründler. *Chemische Sensoren - Eine Einführung für Naturwissenschaftler und Ingenieure*. Berlin/Heidelberg: Springer-Verlag, 2004.

[61] Adam Hulanicki, Glab Stanislaw, and Ingman Folke. “Chemical Sensors Definitions and Classification”. In: *Pure & Applied Chemistry* 63.9 (1991), pp. 1247–1250.

[62] Petra Spitzer. “Traceable measurements of pH”. In: *Traceability in Chemical Measurement*. Berlin, Heidelberg: Springer Berlin Heidelberg, 2001, pp. 206–211.

[63] Petra Spitzer and Kenneth W Pratt. “The history and development of a rigorous metrological basis for pH measurements”. In: *Journal of Solid State Electrochemistry* 15.1 (2011), pp. 69–76.

[64] R Buck et al. “Measurement of pH Definition, Standards, and Procedures”. In: *Handbook of Biochemistry and Molecular Biology, Fourth Edition* 74.11 (2010), pp. 675–692.

[65] Martin Strobl et al. “NIR-emitting aza-BODIPY dyes-new building blocks for broad-range optical pH sensors”. In: *Analyst* 140.21 (2015), pp. 7150–7153.

[66] Cheng-Gang Niu et al. “A ratiometric fluorescence sensor with broad dynamic range based on two pH-sensitive fluorophores”. In: *The Analyst* 130.11 (2005), p. 1551.

[67] Sergey M Borisov et al. “New Life of Ancient Pigments: Application in High-Performance Optical Sensing Materials”. In: *Analytical Chemistry* 85.19 (2013), pp. 9371–9377.

[68] Ingo Klimant et al. *New Trends in Fluorescence Spectroscopy*. Ed. by Bernard Valeur and Jean-Claude Brochon. Vol. 1. Springer Series on Fluorescence January. Berlin, Heidelberg: Springer Berlin Heidelberg, 2001.

[69] Agustin G Asuero and Tadeusz Michałowski. “Comprehensive Formulation of Titration Curves for Complex Acid-Base Systems and Its Analytical Implications”. In: *Critical Reviews in Analytical Chemistry* 41.2 (2011), pp. 151–187.

[70] Reggie S Spaulding et al. “Autonomous in Situ Measurements of Seawater Alkalinity”. In: *Environmental Science & Technology* 48.16 (2014), pp. 9573–9581.

[71] Alejandro N Colli, Hubert H Girault, and Alberto Battistel. “Non-Precious Electrodes for Practical Alkaline Water Electrolysis”. In: *Materials* 12.8 (2019), p. 1336.

[72] Nianjun Yang, Siegfried R Waldvogel, and Xin Jiang. “Electrochemistry of Carbon Dioxide on Carbon Electrodes”. In: *ACS Applied Materials & Interfaces* 8.42 (2016), pp. 28357–28371.

[73] A.L. Yuvaraj and D Santhanaraj. “A systematic study on electrolytic production of hydrogen gas by using graphite as electrode”. In: *Materials Research* 17.1 (2013), pp. 83–87.

[74] Derek Pletcher. “Carbon Electrodes in Electrochemical Technology”. In: *Electrochemistry of Carbon Electrodes*. Ed. by Richard C. Alkire, Philip N. Bartlett, and Jacek Lipkowski. Advances in Electrochemical Sciences and Engineering. Wiley, 2015, pp. 316–317.

[75] György Inzelt. “Pseudo-reference Electrodes”. In: *Handbook of Reference Electrodes*. Berlin, Heidelberg: Springer Berlin Heidelberg, 2013, pp. 331–332.

[76] J.G. Vos and M.T.M. Koper. “Measurement of competition between oxygen evolution and chlorine evolution using rotating ring-disk electrode voltammetry”. In: *Journal of Electroanalytical Chemistry* 819 (2018), pp. 260–268.

[77] J.E. Bennett. “Electrodes for generation of hydrogen and oxygen from seawater”. In: *International Journal of Hydrogen Energy* 5.4 (1980), pp. 401–408.

[78] Marc T.M. Koper. “Thermodynamic theory of multi-electron transfer reactions: Implications for electrocatalysis”. In: *Journal of Electroanalytical Chemistry* 660.2 (2011), pp. 254–260.

[79] Hwan Young Song et al. *Preparation and Characterization of Manganese Dioxide Electrodes for Highly Selective Oxygen Evolution During Diluted Chloride Solution Electrolysis*. Tech. rep. 4. 2007, pp. 545–551.

[80] M.A Rabah, Nabil Nassif, and A.A.Abdul Azim. “Electrochemical wear of graphite anodes during electrolysis of brine”. In: *Carbon* 29.2 (1991), pp. 165–171.

[81] Raluca-Elena Munteanu et al. “Water Electrolysis Carried Out on Microelectrodes to Obtain New Insights into the Regulation of Cytosolic pH”. In: *ChemElectroChem* 6.6 (2019), pp. 1800–1807.

[82] David W.H. Rankin. “CRC handbook of chemistry and physics, 89th edition, edited by David R. Lide”. In: *Crystallography Reviews* 15.3 (2009), pp. 223–224.

[83] C.L. Young. “Hydrogen and Deuterium”. In: *IUPAC-NIST Solubility Database* 5/6 (1981).

[84] R. Battino. “Oxygen and Ozone”. In: *IUPAC-NIST Solubility Database* 7 (1981).

[85] Kenji Kikuchi et al. “Characteristics of hydrogen nanobubbles in solutions obtained with water electrolysis”. In: *Journal of Electroanalytical Chemistry* 600.2 (2007), pp. 303–310.

[86] Kenji Kikuchi et al. “Concentration determination of oxygen nanobubbles in electrolyzed water”. In: *Journal of Colloid and Interface Science* 329.2 (2009), pp. 306–309.

[87] Guanghua Zhao and N. Dennis Chasteen. “Oxidation of Good’s buffers by hydrogen peroxide”. In: *Analytical Biochemistry* 349.2 (2006), pp. 262–267.

[88] Catriona A Collins et al. “Towards multifunctional antioxidants: synthesis, electrochemistry, in vitro and cell culture evaluation of compounds with ligand/catalytic properties”. In: *Organic & Biomolecular Chemistry* 3.8 (2005), p. 1541.

[89] Sławomira Skrzypek et al. “Square wave adsorptive stripping voltammetric determination of famotidine in urine”. In: *Talanta* 66.5 (2005), pp. 1146–1151.

[90] Song Hi Lee and Jayendran C Rasaiah. “Proton transfer and the mobilities of the H + and OH - ions from studies of a dissociating model for water”. In: *The Journal of Chemical Physics* 135.12 (2011), p. 124505.

[91] Ogbonnaya C Okorafor. “Solubility and Density Isotherms for the Sodium Sulfate-Water-Methanol System”. In: *Journal of Chemical & Engineering Data* 44.3 (1999), pp. 488–490.

[92] Beat Müller, Joseph S. Meyer, and René Gächter. “Alkalinity regulation in calcium carbonate-buffered lakes”. In: *Limnology and Oceanography* 61.1 (2016), pp. 341–352.

[93] Frank J. Millero, Kitack Lee, and Mary Roche. “Distribution of alkalinity in the surface waters of the major oceans”. In: *Marine Chemistry* 60.1-2 (1998), pp. 111–130.

[94] Douglas A. Skoog et al. “Aqueous Solutions and Chemical Equilibria”. In: *Fundamentals of Analytical Chemistry*. 2014, pp. 219–222.

[95] Norman E Good et al. “Hydrogen Ion Buffers for Biological Research *”. In: *Biochemistry* 5.2 (1966), pp. 467–477.

[96] Allen J. Bard and Faulkner Larry R. “Potential Sweep Methods”. In: *Electrochemical Methods: Fundamentals and Applications*, p. 231.

[97] S.I. Bailey and I.M. Ritchie. “A cyclic voltammetric study of the aqueous electrochemistry of some quinones”. In: *Electrochimica Acta* 30.1 (1985), pp. 3–12.

[98] May Quan et al. “Voltammetry of Quinones in Unbuffered Aqueous Solution: Reassessing the Roles of Proton Transfer and Hydrogen Bonding in the Aqueous Electrochemistry of Quinones”. In: *Journal of the American Chemical Society* 129.42 (2007), pp. 12847–12856.

[99] Daniel P Tabor et al. “Mapping the frontiers of quinone stability in aqueous media: implications for organic aqueous redox flow batteries”. In: *Journal of Materials Chemistry A* 7.20 (2019), pp. 12833–12841.

[100] Robert J. Forster and Joseph P. O’Kelly. “Protonation reactions of anthraquinone-2,7-disulphonic acid in solution and within monolayers”. In: *Journal of Electroanalytical Chemistry* 498.1-2 (2001), pp. 127–135.

Part IV.

Appendix

A. Cell Parameters

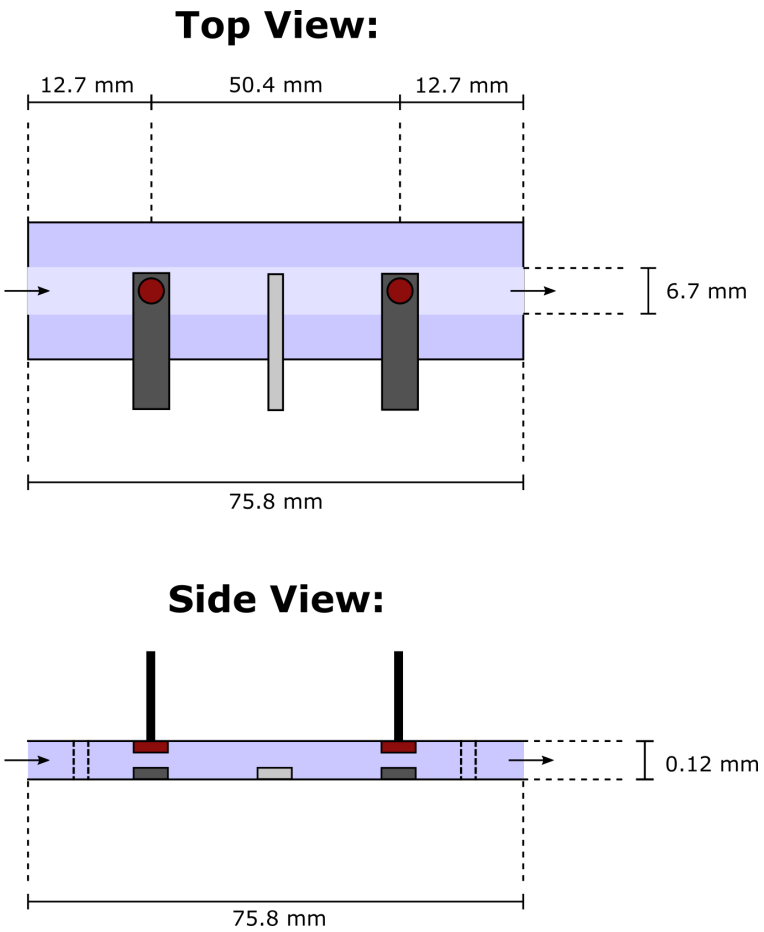

Figure A.1.: Flow cell parameters.

B. Cyclic Voltammetry Studies

2,7-Anthraquinonedisulfonic acid

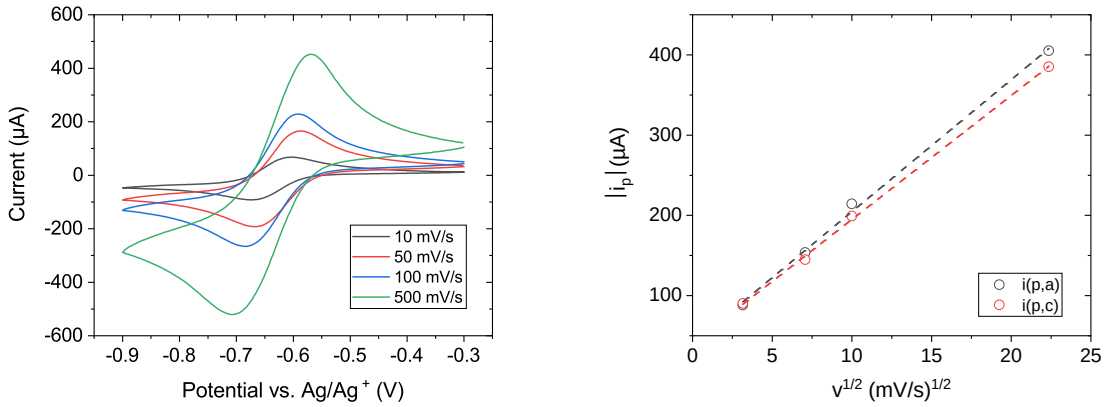

Figure B.1.: CV of 10 mM AQDS in 0.1 M KCl on screen printed gold electrodes (left) and resulting peak current versus square root of scan rate plot (right).

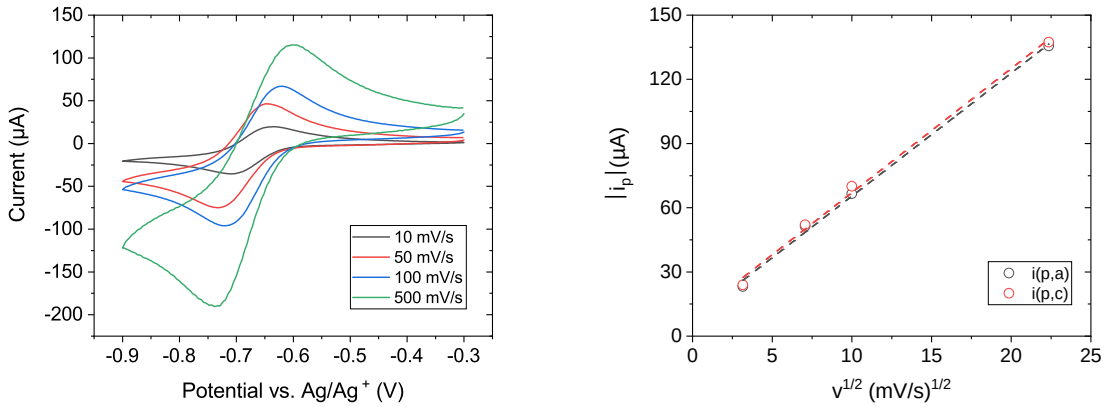

Figure B.2.: CV of 1 mM AQDS in 0.1 M KNO_3 on screen printed gold electrodes (left) and resulting peak current versus square root of scan rate plot (right).

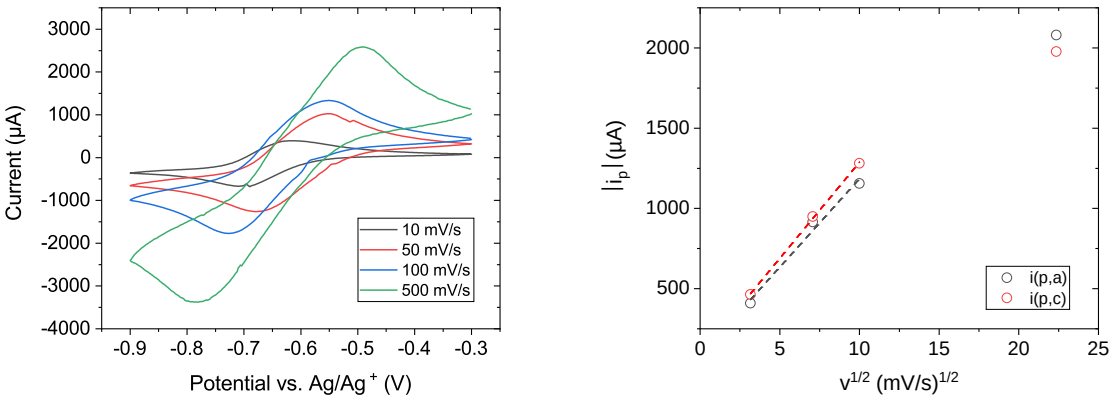

Figure B.3.: CV of 100 mM AQDS in 0.1 M KNO_3 on screen printed gold electrodes (left) and resulting peak current versus square root of scan rate plot (right).

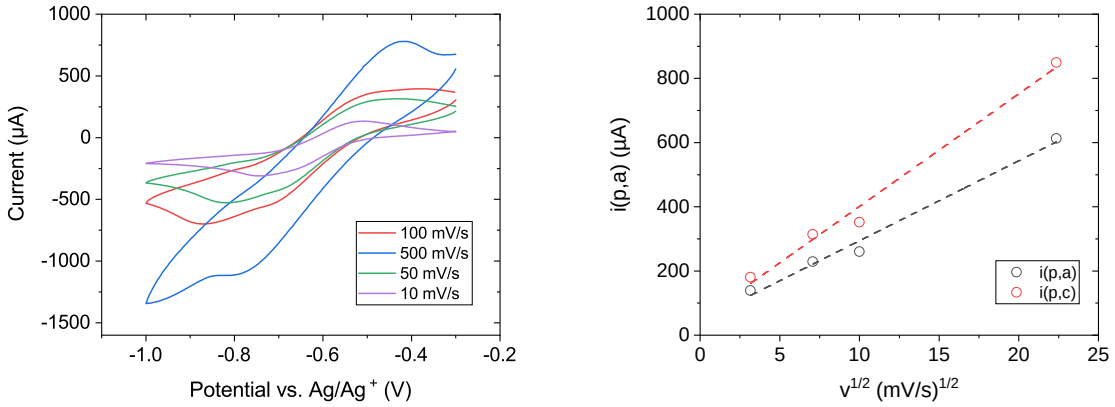

Figure B.4.: CV of 100 mM AQDS in 0.1 M KNO_3 on screen printed carbon electrodes (left) and resulting peak current versus square root of scan rate plot (right).

1,4-Benzoquinone

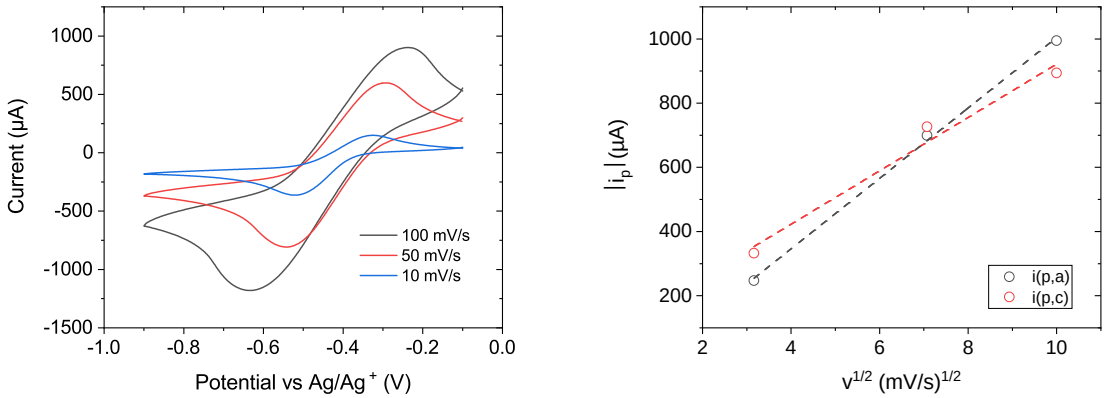

Figure B.5.: CV of 100 mM BQ in 0.1 M KNO_3 on screen printed carbon electrodes (left) and resulting peak current versus square root of scan rate plot (right).

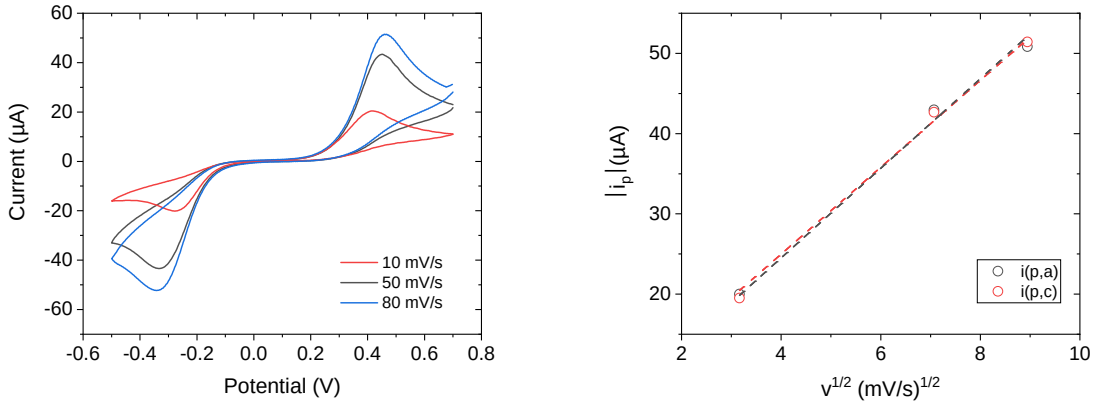

Figure B.6.: CV of 100 mM BQ in 0.1 M KNO_3 on screen printed carbon electrodes (left) and resulting peak current versus square root of scan rate plot (right).

C. List of Figures

D. List of Tables